Chemical Geology 578 (2021) 120213

Contents lists available at ScienceDirect

Chemical Geology

journal homepage: www.elsevier.com/locate/chemgeo

Combined petrography, noble gas, stable isotope and fluid inclusion chemistry of carbonatites from Uganda: Implications for the origin of the carbonatite melt in continental rift setting

Zsolt Benkó [a,*], Kata Molnár [a], Tomáš Magna [b], Vladislav Rapprich [b], László Palcsu [a], Ondřej Pour [b], Bohuslava Čejková [b], István Futó [a], György Czuppon [c]

[a] Isotope Climatology and Environmental Research Centre, Institute for Nuclear Research, Eötvös Loránd Research Network, Bem tér 18/c, H-4026, Debrecen, Hungary
[b] Czech Geological Survey, Klárov 3, CZ-11821 Prague, Czech Republic
[c] Research Centre for Astronomy and Earth Sciences, Eötvös Loránd Reserach Network, Budaörsi út 45, H-1112 Budapest, Hungary

ARTICLE INFO

Keywords:
Sukulu and Tororo carbonatites
Noble gases
Stable isotopes
Fluid inclusions
Mantle
Carbothermal origin

ABSTRACT

An integrated petrographic, fluid inclusion, noble gas, and stable isotope study was performed for the Late Oligocene, spatially associated Sukulu and Tororo carbonatite complexes in SE Uganda in order to understand their genesis and provide additional constraints on the evolution of the East African Rift System (EARS). Both carbonatite complexes comprise mainly ring-shaped calcio-carbonatites with accessory primary magmatic phases, including olivine, phlogopite, aegirine and pyrochlore. Absent or low Na deficiency on the A-site and high F contents (0.4–1.2 *apfu*) reveal the magmatic origin of pyrochlore. In contrast, the corroded rims of olivine, Sr-enrichments of the rims of apatite, as well as the occurrence of Sr- and Mg-rich lamellae in calcite, coupled with the presence of barite, REE-witherite, siderite, pyrite, bastnäsite and galena as secondary phases imply a hydrothermal overprint of the primary magmatic mineral assemblage.

Fluid inclusions found in the cores of clustered apatite crystals are primary, two-phase H_2O + NaCl aqueous inclusions in Sukulu-, and two-, or multi-phase H_2O + NaCl ± $NaHCO_3$ ± other solid inclusions in Tororo Complex. In the gas phase of some inclusions small amounts of CO_2 or CH_4 have been detected by micro-Raman analysis. The estimated trapping temperature of 330–425 °C and pressure of 465–1330 bars using the accepted denudation rates calculated for the EARS as independent barometers, reveal subsolidus crystallization conditions for the intercrystalline clustered apatite aggregates. Stable C-O isotope compositions of both carbonatite complexes suggest ultimately a mantle origin for the carbonate phase.

Helium, neon and argon isotope compositions, liberated by crushing of bulk rock, apatite and calcite samples, show a systematic variation between the analyzed phases. Relatively low $^3He/^4He$ ratios of apatite and pyroxene separates (<5.3 R_a) are accounted for by radiogenic production of ^4He in these minerals, whereas the air-corrected values in calcite reach as high as 9.6 R_a, characteristic for plume sources. Whole-rock Ne isotope ratios provide evidence for a depleted MORB mantle (DMM) trend. Combined $(^{21}Ne/^{22}Ne)_{EX}$ (air-corrected $^{21}Ne/^{22}Ne$ ratio extrapolated to Ne-B composition Holland and Ballentine, 2006; Trieloff et al., 2000) versus $^4He/^3He$ are indicative of mixing of a plume-like and a DMM-like component in the source region of the parental carbonatite magmas, which is in contrast to some recent interpretations of recent/sub-recent magmas in the EARS. Based on new noble gas data from this study we argue that in the early phase of the magmatic activity of the EARS, a low-viscosity carbonatite magma may have intruded into the shallow crust rapidly, without any significant contamination by the sub-continental lithospheric mantle.

Combined fluid inclusion data and noble gas results collectively imply that the carbonatites worldwide are carbothermal (hydrothermal) rather than purely magmatic products and that they crystallized at sub-solidus temperatures from dominantly magma-derived fluids.

* Corresponding author.
E-mail address: benko.zsolt@atomki.hu (Z. Benkó).

https://doi.org/10.1016/j.chemgeo.2021.120213
Received 13 June 2020; Received in revised form 24 March 2021; Accepted 30 March 2021
Available online 1 April 2021

1. Introduction

Carbonatites associated with alkaline silicate ring complexes are the main economic source of Nb and critical metals (Nb: Mackay and Simandl, 2014; Simandl et al., 2018; Simandl and Paradis, 2018; REE: Hou et al., 2015; Simandl, 2014; Verplanck et al., 2016) and are often a significant repository of Cu–Ti–Fe–Au–U–Th (e.g., Palabora Complex: Groves and Vielreicher, 2001), apatite (e.g., Sukulu Complex: McDonald et al., 2010), vermiculite and fluorite (e.g., Speewah Complex: Alvin et al., 2004; Amba Dongar: Palmer and Williams-Jones, 1996). Large rare earth-, precious- and strategic element enrichments associated with carbonatites are, however, confined to carbonatites that originate from refertilized subcontinental lithospheric mantle (SCLM: Hou et al., 2015; Kumar et al., 1998; Schleicher et al., 1998). An additional prerequisite is a thick lithosphere and/or high pressure (~25 kbar) and favorable pathways (translithospheric faults) for magma ascending into the overlying crust. Favorable regions are the thickened continental margins above ancient subduction zones with thick metamorphic sequences (e.g., Bayan Obo, Maoniuping, Dalucao, Lizhuang deposits in China; Hou et al., 2015).

Based on isotope evidence (Pb/Pb; Sr/Nd; stable O and C isotopes; noble gas isotope systematics) there is a general consensus about the mantle origin of primary magmatic carbonatites (Bell and Simonetti, 2010; Guzmics et al., 2012; Guzmics et al., 2011; Kjarsgaard, 1998; Kjarsgaard et al., 1995) although carbonatites of crustal origin were also reported (Ferrero et al., 2016; Lustrino et al., 2019). Although carbonatites themselves are generally considered as magmatic products, a significant part of carbonatite-related mineralizations is associated with 'carbohydrothermal' deposits. The term 'carbohydrothermal' or 'carbothermal residua' has been introduced by Mitchell (2005) and Woolley and Kjarsgaard (2008), and is generally thought to represent carbonatites which precipitated at subsolidus temperatures from CO_2–H_2O- and/or H_2O-rich fluids (Simandl and Paradis, 2018).

The isotope systematics of noble gases and fluid inclusions have been rarely studied in carbonatites and these studies mainly focus on constraining the source regions of the carbonatites (e.g., Buikin et al., 2014; Hopp and Viladkar, 2018; Murty et al., 2007; Sasada et al., 1997; Lustrino et al., 2020; Mata et al., 2010). An integrated approach, including rock petrography, mineral chemistry, fluid inclusion microthermometry combined with the chemical and isotope analysis of the fluid inclusion assemblages entrapped in various mineral phases of carbonatites may provide additional constraints on the formation and post-emplacement history of these rocks, with implications for hydrothermal conditions and mobility of REE and other critical metals. We provide new mineralogical and geochemical data (major and trace element chemistry, stable C-O compositions, He–Ne–Ar elemental and isotope systematics) of two carbonatite complexes at Sukulu and Tororo (SE Uganda), with a particular focus to highlight the significance of the fluids in the formation of the carbonatites in the East African Rift System (EARS). We also evaluate the economic potential (REE) of these two carbonatite occurrences in light of the geochemical evolution, and the genetic and geodynamic position of Sukulu and Tororo deposits during the Late Paleogene.

2. Geological setting of Sukulu and Tororo carbonatite bodies

The Sukulu and Tororo carbonatite twinned complexes in southeastern Uganda belong to the southern part of the EARS between the Kenyan and Western Rift segment within the Kenyan Dome (Fig. 1a; Ernst and Bell, 2010). The EARS is the youngest (Eocene to Recent) major Large Igneous Province (LIP) that is stretching in S-N direction from Malawi to the Red Sea and Gulf of Aden. The EARS formed above the African Superplume having two heads, the Ethiopia and Kenya domes (George et al., 1998; Halldórsson et al., 2014). Owing to the

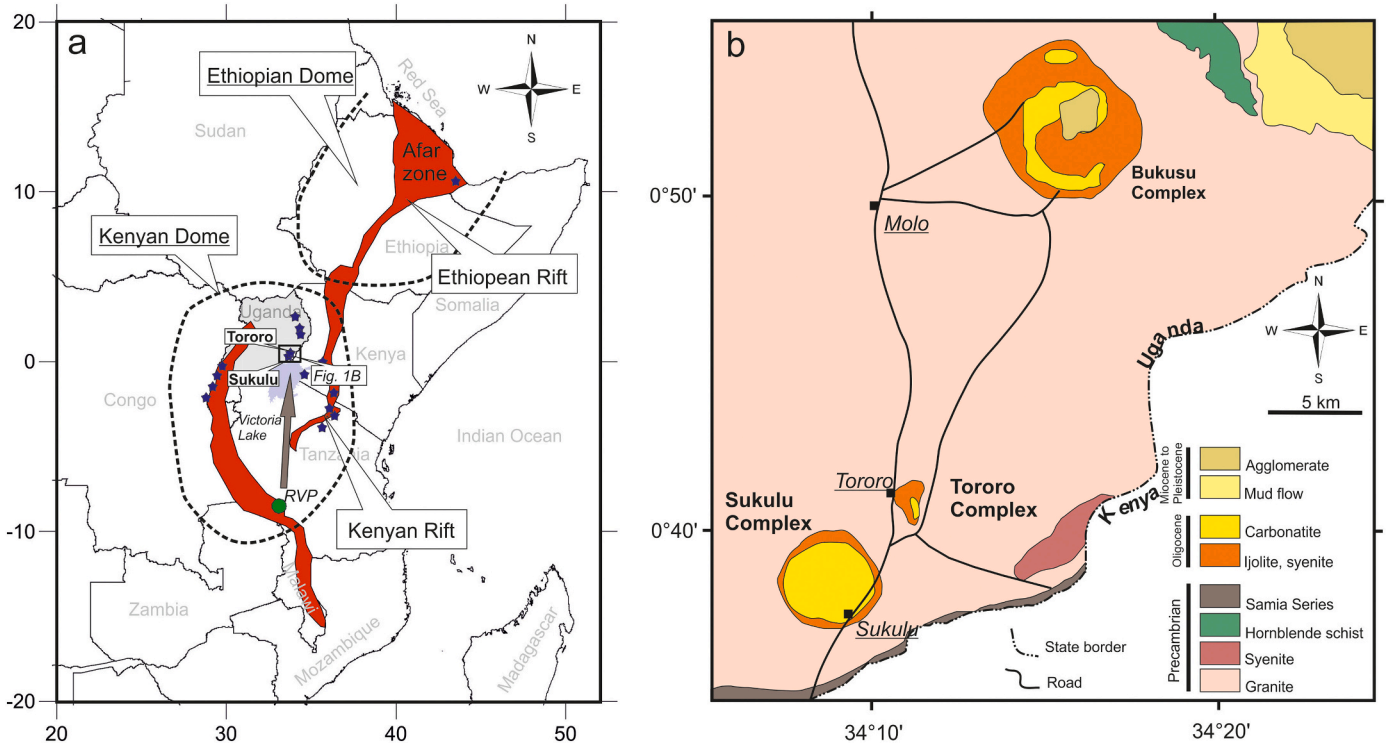

Fig. 1. **a**, East African Rift System. The stars indicate the alkaline carbonatite ring complexes in an offset position compared to the locus of the main alkali basalt volcanism (red-colored field). The paleogeographic position of Sukulu and Tororo corresponds to the current location of the Rungwe Volcanic Province in Tanzania. The gray arrow indicates the ca. 1000 km northward shift of Africa. Abbreviations: RVP – Rungwe Volcanic Province (current position). **b**, Geological sketch map of SE Uganda showing the Sukulu and Tororo complexes. Modified after Raja and Vise (1973)). (For interpretation of the references to colour in this figure legend, the reader is referred to the web version of this article.)

northern shift of the African continent, currently the center of the active doming is in the Afar Region forming a triple rift junction and causing the rifting of the Red Sea and the Gulf of Aden (Courtillot et al., 1999; Ernst and Bell, 2010). Igneous activity in the EARS is dominated by alkali flood basalt magmatism whilst carbonatite magmatism is only subordinate in volume. The carbonatites and associated alkaline silicate rocks accompany the rift valley and are currently in offset position, located along the eastern and the western margins of the Kenyan Dome on the Archean craton (Fig. 1a; Ernst and Bell, 2010). During the Palaeogene, the two complexes were situated ca. 1000 km south from their current position, in a more axial position. Carbonatite and associate alkaline silicate rocks (melteigite, ijolite, nepheline syenite) of Sukulu and Tororo complexes form dissected ring-shaped bodies with diameters of ~4 km and ~ 1 km, respectively (Fig. 1b). Both complexes are surrounded by fenitized granitic-gneissic bedrock.

2.1. Sukulu

The Sukulu carbonatite complex (Fig. 1.b) has been under intense exploration since the 1960's for its large Nb, fluorapatite and magnetite resources that are concentrated mainly in the residual soils covering the carbonatite intrusion (Mitchell, 2005; Reedman, 1984). The Sukulu complex was dated at 24–26 Ma (K–Ar; Bloomfield, 1973; Davies, 1965), thus belonging to the oldest carbonatite intrusions of the EARS. The intrusion is surrounded by alkaline silicate rocks (mainly ijolite) and fenitized granitic–gneissic bedrock. The carbonatite is mainly a white-colored coarse grained calcio-carbonatite (sövite) with 70–95% calcite but subordinate ankeritic and dolomitic carbonatites and carbonatite breccia also occur as late phases. Common accessory minerals are apatite, magnetite, biotite, zircon, pyrochlore and baddeleyite (Notholt et al., 1989). Ting et al. (1994b) distinguished CO_2-, CH_4- and H_2O-bearing fluid inclusions in apatite. According to their interpretation, H_2O and CO_2 fluids formed by fluid immiscibility at high temperatures and pressures (>1000 °C, 7.4 kbar). The deep magmatic fluids developed further to hydrothermal p–T conditions and H_2O–CH_4-dominated fluid inclusions trapped at shallow depth and temperature (~500 °C, <3 kbar).

2.2. Tororo

The Tororo carbonatite body, ~2 km northeast of Sukulu (Fig. 1b), has been mined since 1953 for the cement industry; however, apatite and magnetite may also form the economic concentrations (Mineral, Mining sector investment and Business Guide Vol. 1. Uganda). The carbonatite complex comprises a sövite plug rising ~300 m above the Uganda Basement Complex and is surrounded by brecciated ijolite, nepheline syenite and syenitic fenite. The carbonatite and the alkaline silicate rocks are intersected by a succession of 1 cm to 1 m thick magnetite- and locally fluorite-bearing fine-grained calcio-carbonatite (alvikite) veins and dykes. Fluid inclusion studies of Rankin (1977) showed that fluids trapped in apatite are alkali-rich [nahcolite ($NaHCO_3$)-bearing] aqueous inclusions with homogenization temperatures of up to 365 °C. Rankin (1977) also concluded that the apatite formed under subsolidus temperatures and that carbonatite has a 'carbothermal' origin.

3. Sampling and analytical methods

3.1. Bulk-rock composition and mineral chemistry

The samples from Tororo and Sukulu were collected during two Czechoslovak expeditions in 1970's and stored since in the repository of the Czech Geological Survey. Following crushing and pulverizing in an agate box, major element concentrations were determined at the Czech Geological Survey using conventional wet chemistry procedures, outlined in Dempírová et al. (2010). Whole-rock trace element contents were acquired by employing an Agilent 7900× ICPMS, following dissolution in 15 M HNO_3–23 M HF and equilibration in 6 M HCl.

In situ mineral chemistry and particularly the distribution of critical elements among the coexisting mineral phases of the studied rocks were analyzed using a FEG-SEM Tescan MIRA 3GMU, equipped with EDX microanalysis system Oxford Instruments X-Max 20, housed at the Czech Geological Survey. EDX analyses were conducted with an accelerating voltage of 15 kV, beam current of 3 nA, working distance 15 mm and counting time of 15 s. A combination of natural and synthetic standards was used for calibration. Analyses were processed using the AZtec software (Oxford Instruments).

3.2. Fluid inclusion microthermometry and micro-Raman analysis

Double-polished thin sections were prepared to select the key samples for fluid inclusion studies and noble gas analysis. Based on the petrographic observations samples rich in fluid inclusions and free of other mineral inclusions were selected. The fluid inclusion studies were carried out at the Department of Mineralogy, Geochemistry and Petrology, University of Szeged, using a Linkam THMSG600 heating–freezing stage mounted on an Olympus BX41 microscope. Calibration of the heating–freezing stage was carried out using synthetic inclusions of pure H_2O [T_m(ice) = 0.0 °C, T_h(crit) = 374 °C] and H_2O–CO_2 inclusions [$T_m(CO_2)$ = −56.6 °C] entrapped in quartz.

Raman spectroscopy was performed at the Department of Mineralogy, Geochemistry and Petrology, University of Szeged, by employing a Thermo Scientific DXR Raman microscope equipped with a diode-pumped frequency-doubled Nd-YAG laser at 10 mW maximum laser power. The samples were irradiated by laser light at a wavelength of 532.2 nm, with the laser beam focused using a 100× objective lens, resulting in a spot size of ca. 0.7 μm. The backscattered light collected by the microscope objective was filtered through an edge filter, dispersed by a single grating (900 grooves mm^{-1}), and gathered in a CCD detector cooled to −20 °C by the Peltier cooling device. The instrument had a spectral resolution better than 4 cm^{-1} and a spatial resolution of a few μm^3; a 50 μm pinhole confocal aperture was used for each measurement. All spectra were recorded with 10 mW laser power.

3.3. Noble gas elemental and isotope analysis

Noble gas isotope analyses were carried out at the Institute for Nuclear Research, Debrecen, Hungary. The selected rock samples were gently crushed into 0.1–5.0 mm pieces. Apatite was separated from calcite by heavy liquid (sodium polytungstate) separation, by setting the density of the liquid to 2.75 g × cm^{-3}. Thus, besides of whole-rock samples, calcite, apatite and pyroxene separates were also prepared. Following this procedure, both whole-rock samples and mineral separates were cleaned in acetone ultrasonic bath and dried at 60 °C overnight to remove any adhering contamination. Approximately 100 mg of calcite, pyroxene and apatite mineral separates as well as whole-rock aliquots were loaded into a stainless steel tube attached to the vacuum line. The mineral separates were crushed in an ultrahigh-vacuum stainless steel chamber. The gas was extracted by crushing with the piston which was activated using an external magnet. In addition to single crushing experiments (100 strokes on whole-rock samples and mineral separates), stepwise crushing was applied for whole-rock samples (two steps included 50 and 150 strokes). Different components of the released gas were separated in a cryogenic system consisting of two cold traps and a getter trap. Argon, and the chemically active gases (e.g., O_2, CH_4, CO_2, etc.) were adsorbed in an empty trap at 25 K. Thereafter, He and Ne were adsorbed in a charcoal trap at 10 K. Helium and Ne were desorbed at 42 and 90 K, respectively, whereas Ar was desorbed from the trap at 55 K. The isotope compositions of each noble gas were measured sequentially after purification in a getter trap (SAES) using a HELIX-SFT noble gas mass spectrometer (He) and VG 5400 noble gas mass spectrometer (Ne, Ar), respectively. Signals were collected using a

Faraday cup (^{4}He in the HELIX-SFT and ^{40}Ar in the VG5400) and an electron multiplier for all other isotopes of interest. The overall measurement procedure was calibrated with known air aliquots and calibration gases. The measured He isotope ratios have been corrected for excess air using the atmospheric ^{3}He/^{4}He and ^{4}He/^{20}Ne ratios, recommended by Ballentine et al. (2002). The corrections resulted in very minor changes (0.01%) of the final data.

3.4. Stable C-O isotope measurements

Carbon and oxygen stable isotope ratios in calcite samples were measured at the ICER Centre, Institute for Nuclear Research, Debrecen, Hungary using a Thermo Finnigan DeltaPLUS XP IRMS combined with a Thermal Combustion/Elemental Analyzer interface. The standard materials IAEA-C08, IAEA-603 and IAEA-LSVEC were measured after the measurement of every seven unknown samples. The measured values are expressed in the delta notation as δ^{13}C relative to V-PDB and δ^{18}O relative to V-SMOW. The external precision of the stable isotope measurements, determined from replicate measurements of reference materials is ±0.1‰ and ± 0.5‰ (1σ) or better for δ^{13}C and δ^{18}O, respectively. In addition, six samples were also analyzed at the Czech Geological Survey, using the procedure of selective decomposition of carbonate (see McCrea, 1950) and by employing a dual inlet Delta V Advantage IRMS (Thermo Fisher). The external reproducibility of the measurements was better than ±0.04‰ for both C and O isotope compositions. The results for reference materials NBS-18 (IAEA) and JLs-1

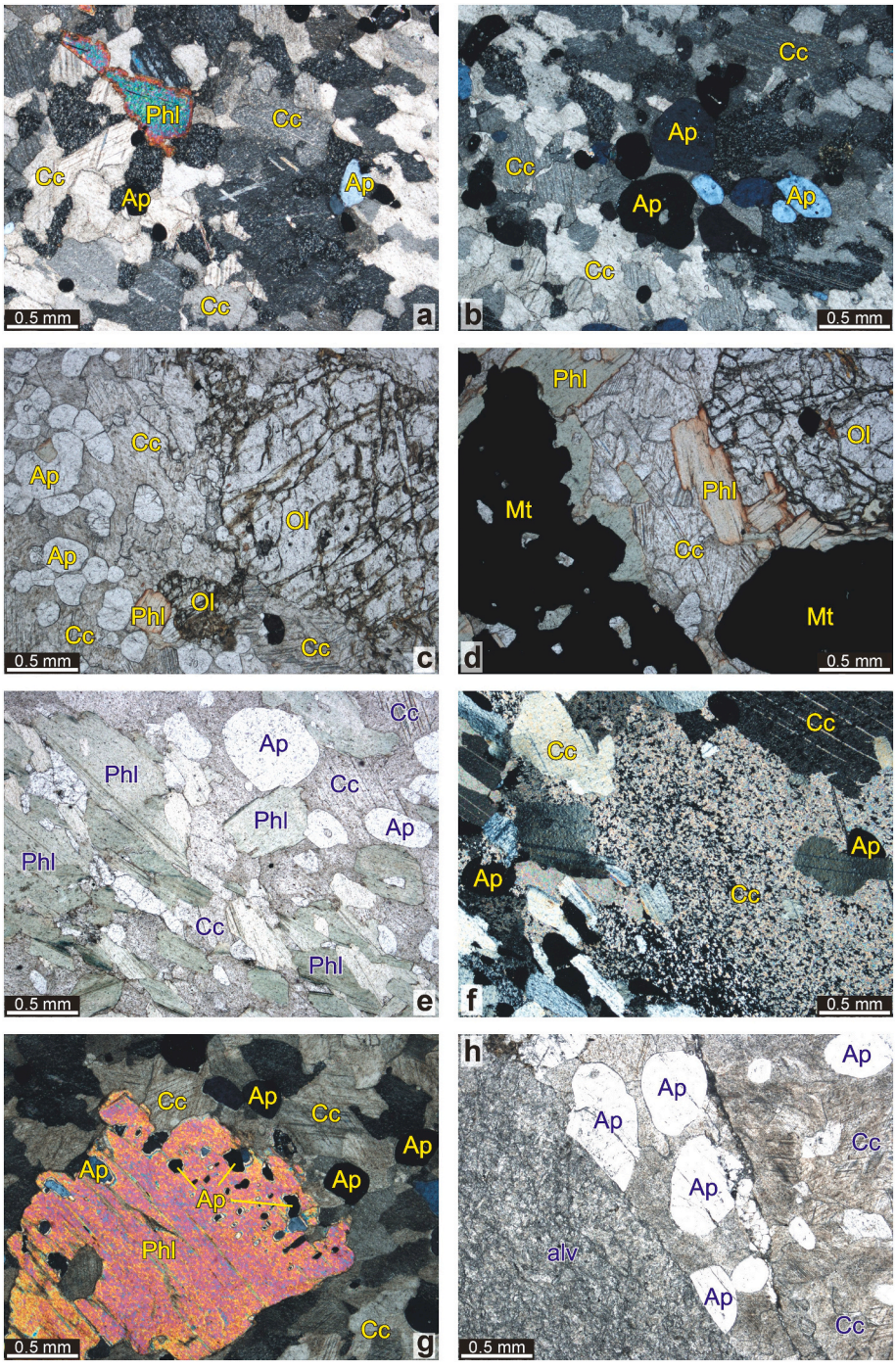

Fig. 2. Microphotographs of samples from the Sukulu complex: **a, b**, Phlogopite-apatite sövite AC01A (cross-polarized light); **c, d**, Olivine-rich phlogopite–apatite sövite with large phenocrysts of magnetite AC01C (plane-polarized light); **e**, Phlogopite–apatite sövite AC01E (plane-polarized light); **f**, Sieve-textured calcite in the phlogopite–apatite sövite AC01E (cross-polarized light); **g**, Poikilitic phlogopite enclosing apatite grains in apatite sövite AC01F (cross-polarized light); **h**, Apatite sövite ACO1F crosscut by alvikite (plane-polarized light). alv – alvikite; Ap – apatite; Cc – calcite; Mt – magnetite; Ol – olivine; Phl – phlogopite.

(Geol. Surv. Japan) are listed in Table 2 and consistent with the published values within the uncertainty (e.g., Ackerman et al., 2017; Daëron et al., 2019). Advantages of the DI-IRMS method over the continuous flow technique are discussed in Trubač et al. (2019).

4. Results

4.1. Petrography and mineral chemistry

The samples from Sukulu complex comprise four sövites AC01A, AC01C, AC01E and AC01F. AC01A is a phlogopite–apatite sövite, in which the oval grains of apatite (~0.1 mm, occasionally up to 0.5 mm) are randomly distributed among equigranular (mostly ~0.5 mm) phaneritic mass of calcite (with small amounts of Mg [0.7–1.1 wt% MgO] and Sr [0.4–0.6 wt% SrO]) grains (Fig. 2a). Nests of larger apatite grains occurs locally (Fig. 2b). Dolomite (with small amounts of Fe [1.9–2.1 wt % FeO]) occur rarely among dominant calcite. Phlogopite (0.5–1 mm) has optically distinct zoning with green cores and pale brown rims. Despite the significant optical difference, both zones differ only little in chemical composition. The rims are slightly more magnesian [molar Mg/(Mg + Fe) = 0.89–0.92] compared to cores (0.87–0.88).

Sample AC01C has relatively abundant large olivine phenocrysts (>5 vol%, 3–5 mm in diameter; Fig. 2c). Olivine ($Fo_{86–88}$) is fresh, with slight alteration apparent solely along the cracks. Irregular grains of magnetite reach a similar size as olivine, but occur more rarely (Fig. 2d). They are mantled with randomly oriented crystals of phlogopite (Fig. 2d). Phlogopite is also scarcely dispersed throughout the rock (Fig. 2c). The olivine and magnetite phenocrysts are surrounded by a phaneritic mass of equigranular calcite (containing small amounts of Mg and Sr) with abundant rounded grains of apatite (0.2–0.5 mm in diameter) and rare dolomite (with Fe).

Sövite AC01E consists of a mixture of equigranular calcite (with small amounts of Mg and Sr) grains (0.5 mm) with rounded apatite grains (0.2–0.5 mm) enclosing the bands of greenish phlogopite, comparable with phlogopite cores in sample AC01A. Mica displays strong preferred orientation parallel with the bands (Fig. 2e), most likely reflecting flow foliation (flow banding). Dolomite, which is more common compared to samples AC01A and AC01C and which contains small amounts of Fe and Mn, displays a sieve-texture (Fig. 2f), suggesting post-crystallization resorption/recrystallization.

Sövite AC01F is also dominated by carbonates with rounded apatite (0.2–0.5 mm). Calcite (with 0.5–1.5 wt% SrO) is predominant with rare dolomite, whereas siderite is present only in a close association with pyrite, possibly representing its alteration product. This sample also includes poikilitic phlogopite (3 mm) enclosing microcrysts of apatite (Fig. 2g) and is crosscut by a dyke of alvikite (Fig. 2h). According to the texture (cut off apatite grains), the alvikite was emplaced into solidified sövite. Some grains of apatite among porphyritic calcite crystals have irregular rims with elevated Sr contents (~0.7 wt% SrO). Pyrite and rare microcrysts of an unidentified Mg–REE phosphate phase were detected on the boundaries between apatite and carbonate in AC01F. Based on electron microscopy (back-scattered electron imaging complemented with EDAX analyses), the alvikite contains more abundant dolomite, but also bastnäsite, barite and sphalerite with galena inclusions.

The main difference between sövites from Sukulu and Tororo (AC03B, AC03C, AC03I) is the presence of aegirine in the latter complex, whereas phlogopite (+olivine) represent the major silicate phases in Sukulu carbonatites. The prevailing carbonate phase of sövite AC03B is calcite with strontianite lamellae. Calcite forms up to 3 mm large crystals, enclosing randomly distributed green aegirine (Fig. 3a). Apatite occurs as rounded crystals forming multicrystalline sutures or clusters occurring exclusively between calcite crystals. Phenocrysts of aegirine (2 mm) enclose pyrite, which is sideritized along cracks, and rarely also pyrochlore. Pyrite contains inclusions of REE-rich witherite (Ba-carbonate). Locally, K-feldspar formed on the rims of aegirine. An identical composition was also observed for sample AC03C (Fig. 3b). In contrast, sövite AC03I has a simpler association, where calcite is associated with apatite (Fig. 3c). This sample includes a contact of carbonatite with apatite–magnetite-rich pyroxenite and breccia (Fig. 2d), but the exact relationships between these individual rock types remain unclear due to a limited size of the sample.

The skeletal Sr-enriched rims of apatite and similar skeletal apatite in

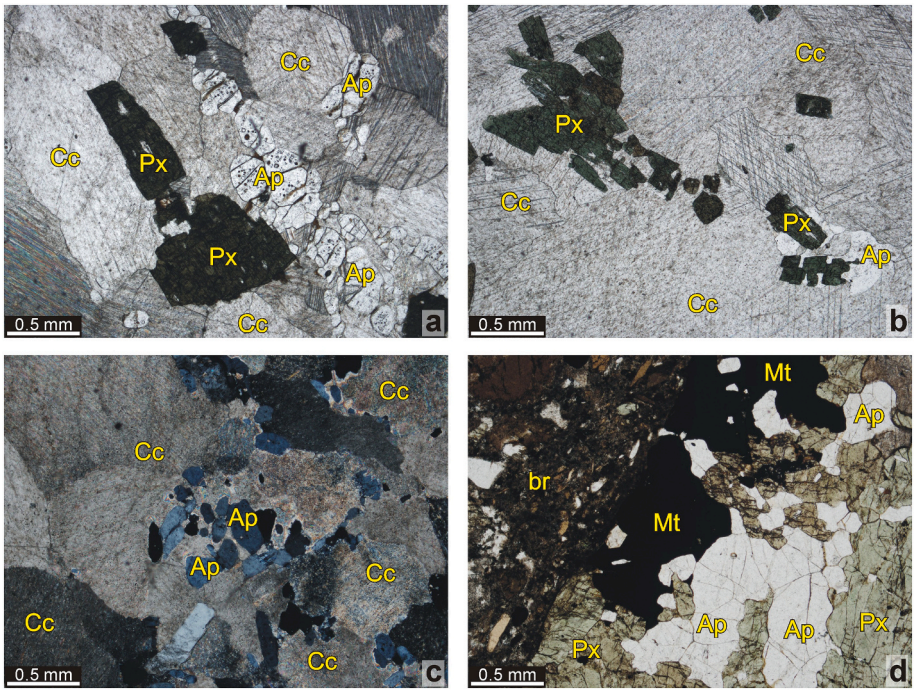

Fig. 3. Microphotographs of samples from the Tororo complex: **a**, Aegirine–apatite sövite ACO3B (plane-polarized light); **b**, Aegirine–apatite sövite AC03C (plane-polarized light); **c**, Apatite sövite AC03I (cross-polarized light); **d**, Apatite-rich pyroxenite probably as a fragment in breccia forming with apatite sövite in sample AC03I (plane-polarized light). br – breccia; Ap – apatite; Cc – calcite; Mt – magnetite; Px – pyroxene (aegirine).

groundmass identified in samples AC01C, AC01E, AC01F and AC03I (Fig. 4) are consistent with post-magmatic hydrothermal overprint of the rocks. Pyrochlore is another mineral phase crystallizing in Nb-rich carbonatites over a wide range of conditions from magmatic and hydrothermal to supergene, and providing valuable data on the rock evolution (e.g., Magna et al., 2020; Nasraoui and Bilal, 2000; Zurevinski and Mitchell, 2004). Rare grains of pyrochlore were detected in sample AC03A, displaying variable compositional zonation (Fig. 5). All analyzed pyrochlores are classified as pyrochlore s.s. within the pyrochlore group according to Hogarth, 1977; Fig. 6a), but compositionally contrasting cores of the heterogeneous grains (grains a and c in Fig. 5) do not correspond to pure pyrochlore. Their increased silica content (Fig. 6b) is combined with depletion in Nb and Na (Fig. 5). Deficiency in Na produces a vacancy on the A-site if calculated according to pyrochlore stoichiometry (Fig. 6c), although some Ba also enters the A-site (Fig. 6d). The compositionally less contrasting cores (grain b in Fig. 5) as well as the rims of all specimens have a similar composition (Figs. 5 and 6), only with increased Ti/Nb value in these less contrasting cores. Even the outermost rims have absent or low A-site vacancies (Fig. 5c and e) suggesting a magmatic origin of these crystals, without significant hydrothermal overprint. The non-stoichiometric cores may represent a mixed structure of pyrochlore partly pseudomorphing after the pre-existing silicate phase. Both non-stoichiometric (mixed structure?) and stoichiometric (pure pyrochlore) cores display elevated contents of U (0.18–0.3 and 0.2–0.42 apfu, respectively; Fig. 6f).

4.2. *Whole-rock chemical compositions*

Whole-rock major and trace element contents are given in Table 1. The MgO and FeO concentrations are below 11.3 wt% and 3.7 wt%, respectively, whereas the CaO contents range 39.3–54.9 wt%. The prevalence of calcite together with coarse-grained texture classify the

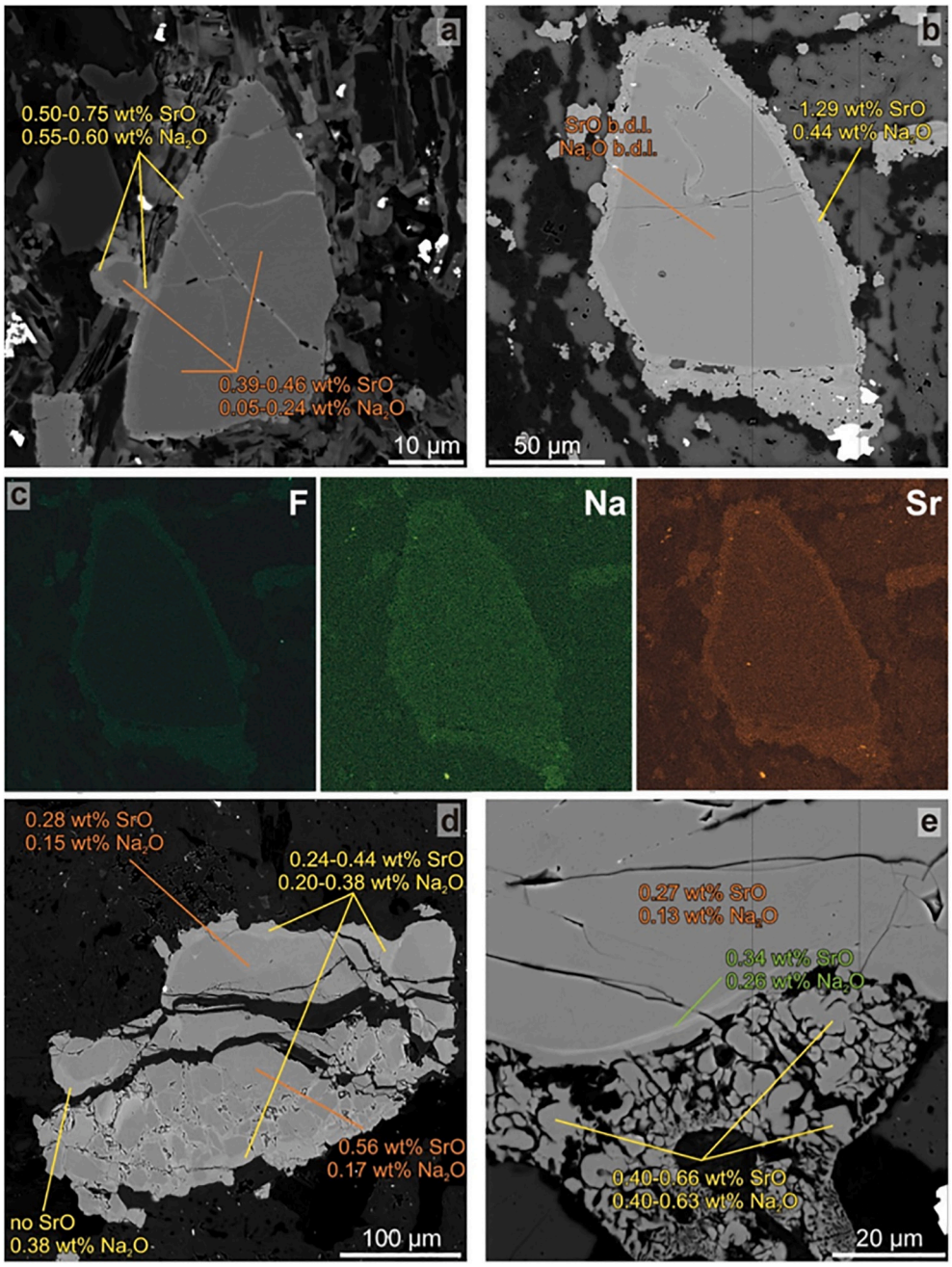

Fig. 4. Apatite grains with visible post-magmatic skeletal Sr-rich rims: **a**, AC03I; **b**, AC01F; **c**, AC01F - distribution maps (F, Na, Sr); **d**, AC01E; **e**, AC01C.

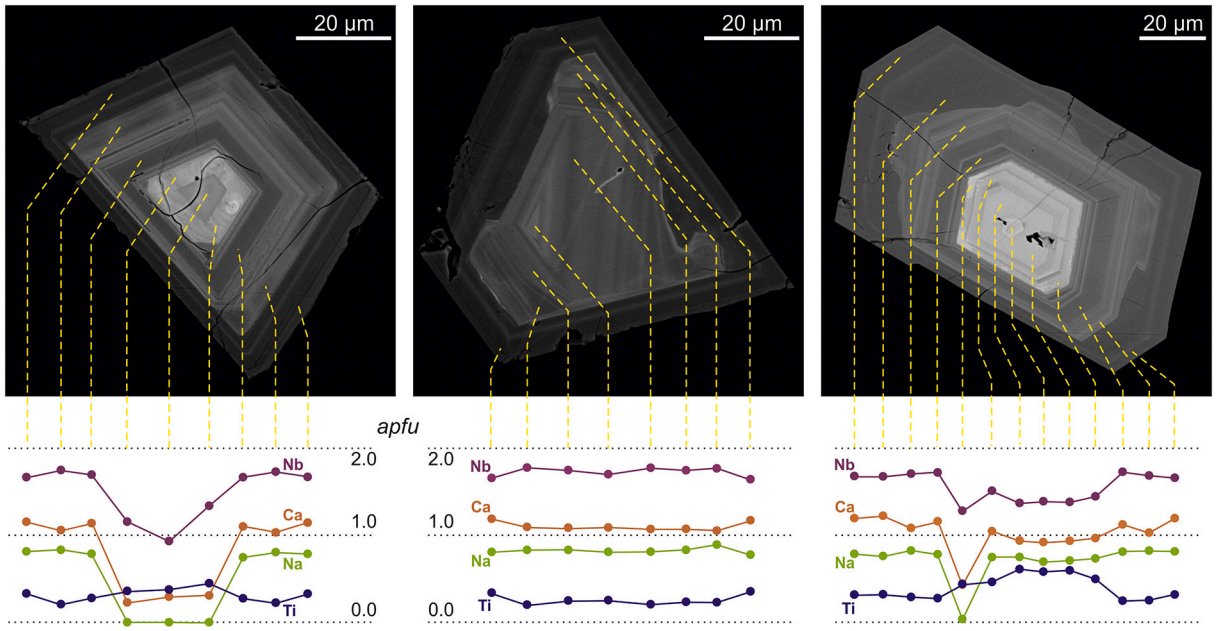

Fig. 5. Compositional maps and profiles of pyrochlore grains from sample AC03C.

studied carbonatites as sövites. The relatively high P_2O_5 content (0.03–4.7 wt%) of the samples is due to the high modal abundance of apatite.

The REE concentrations in samples from Sukulu (803–1208 ppm) and Tororo (547–982 ppm) are lower (ΣREE = 547–1208 ppm) compared to the average REE concentrations of worldwide pristine carbonatites (Woolley and Kempe, 1989). Sövite AC01F shows elevated contents of REE, Zn, Nb, Ba, Pb and U, whereas it has the lowest Zr and Hf contents compared to all other samples from this study. Sövite AC03C has high Th content of 28.4 ppm. The chondrite-normalized patterns show broadly similar trends for both carbonatite bodies (Fig. 7a). The LREE/HREE ratios (La_N/Yb_N = 33–74) are similar to other calcio-carbonatites worldwide (Woolley and Kempe, 1989). The only general difference between the two complexes are the higher V and Sr contents in the Tororo suite compared with Sukulu samples. Individual primitive mantle-normalized patterns are plotted in Fig. 7b. The REE-enriched sövite AC01F (Sukulu) shows the greatest extent of Zr-Hf depletion (in particular Zr) but no depletion in Pb, contrary to all other samples. Sövite AC03C displays excess Th, unlike all other samples. Sövites AC01F, AC03B and AC03C show relative Nb enrichments over Ta whereas sövites AC01A, AC01C and AC01E show the opposite behavior. Niobium, Cd and LREE contents correlate positively with MnO but with no other major element. In the ΣREE vs. Sr/Ba plot (Fig. 7c), the Sukulu carbonatite samples plot in the field of barren carbonatites whereas the Tororo carbonatites plot partly into the mineralized field due to the lower Sr/Ba ratios (1−10) and higher ΣREE concentrations.

4.3. Fluid inclusions and micro-Raman analyses

Fluid inclusions are mainly found in the cores of the apatite crystals (Fig. 8). The negative crystal shaped inclusions in apatite commonly are oriented parallel with the *c* axis of the crystal. They form clusters or appear as single inclusions and are therefore considered as primary inclusions (Fig. 8). Secondary fluid inclusions were not observed in this sample. The following fluid/solid inclusion types (Type I–III) can be distinguished based on visual observations whereby Type I fluid inclusions dominate. (i) Type I inclusions are two-phase aqueous liquid + vapor (L_{aq} + V) inclusions (Fig. 8c). Based on visual estimation at room temperature, the proportion of the vapor phase is 40 vol% and the liquid to vapor ratio is constant. (ii) Type II fluid inclusions have a liquid + vapor + solid (L + V + X_1 ± X_2) composition with a vapor phase proportion of ~40 vol%. The solid phases are anhedral, transparent and optically birefringent. Raman analysis of the solid phases indicates the presence of nahcolite ($NaHCO_3$), calcite ($CaCO_3$) and ankerite [Ca(Fe, Mg, Mn)$(CO_3)_2$] in some multiphase inclusions. In the gas phase of one inclusion CO_2 was detected in trace amounts. (iii) Type III inclusions are optically slightly birefringent, pale pink or green with a solid phase only. Using micro-Raman spectroscopy analysis they were identified as calcite ($CaCO_3$), rhodochrosite ($MnCO_3$), and smithsonite ($ZnCO_3$) (Fig. 8).

In the vapor phase of the Type I inclusions from Tororo minor amounts of CH_4 or CO_2 were detected by micro-Raman spectroscopy. The distance between the hot band of the CO_2 (Fermi doublet) in the two-phase inclusions is 103 cm^{-1} indicating a trace amount of ~0.2 g. cm^{-3} CO_2 (Frezzotti et al., 2012) in these inclusions.

4.4. Microthermometry of fluid inclusions

Two-phase (L + V) Type I inclusions in the apatite homogenized into a liquid phase at temperatures of 278–364 °C in Sukulu samples with a median temperature at ~310 °C (Fig. 9a). Considering the eutectic melting temperatures of ice around −21.2 °C their composition can be modeled in the NaCl–H_2O system. Final melting temperatures of the ice are distributed between −9.6 and −13.8 °C corresponding to 13.5–17.6 NaCl equiv. wt% salinities (Fig. 9b; Bodnar, 1993).

Final homogenization temperatures of Type I (L + V) inclusions into a liquid phase for Tororo samples range from 222 to 342 °C and their distribution has two maxima at ~310 °C and ~ 270 °C, respectively (Fig. 9a). Eutectic temperatures were detected between −21.0 and −27 °C, again indicating a NaCl–H_2O system. Salinities range from 3.7 to 5.3 NaCl equiv. wt% calculated from the melting of the ice phase observed from −5.3 to −3.7 °C (Fig. 9b). Melting of the solid phase in the Type II inclusions (L + V + S) in Tororo samples occurred between 138 and 171 °C, and the median of the final homogenization temperatures was around 270 °C (Fig. 9a).

4.5. Stable C-O isotope compositions

The new $\delta^{18}O$ and $\delta^{13}C$ values obtained in this study are listed in Table 2. The samples show a narrow range of $\delta^{18}O$ values from +7.39 to +8.88‰ and $\delta^{13}C$ values between −3.9 and −0.9‰ (Table 2, Fig. 11).

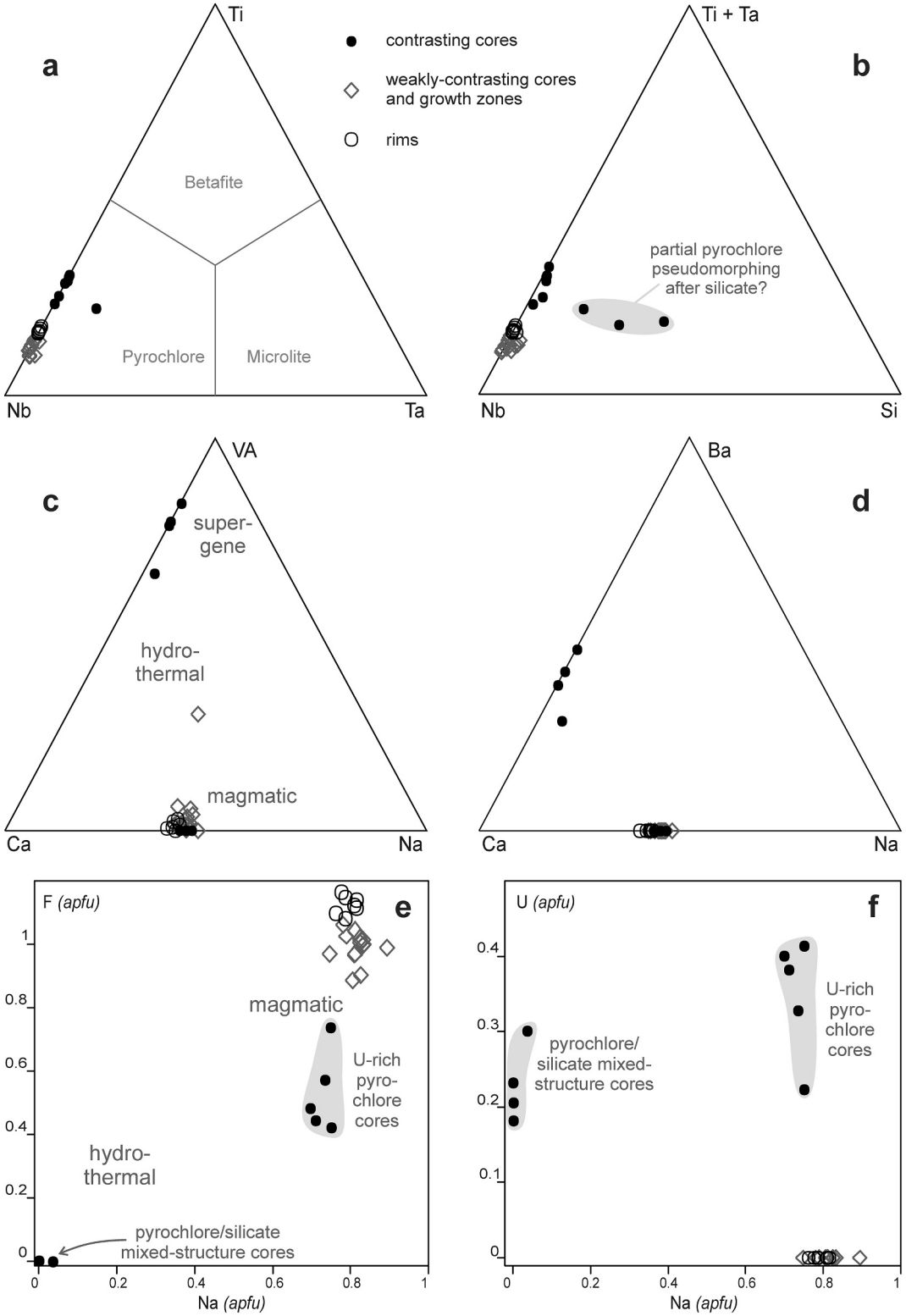

Fig. 6. Classification and compositional diagrams of pyrochlore. VA - Vacancy Site.

Full replicate analysis of sövite AC01C returned identical values within the analytical uncertainty for both $\delta^{18}O$ and $\delta^{13}C$. The difference between DI-IRMS (used at CGS) and EA-IRMS (used at INR) was between −0.17 and + 0.10‰ for $\delta^{13}C$ while it varied between −0.61 and + 0.05‰ for $\delta^{18}O$. This range of relative variations between the two techniques employed is in accord with the observations of Trubač et al. (2019). The $\delta^{18}O$ values fall within the field of primary igneous carbonatites whereas $\delta^{13}C$ values are slightly above this field (Fig. 11); sövite AC01F shows elevated $\delta^{13}C = -1.1$‰, more than 2‰ higher than the other samples from this study. The new values obtained in this study are broadly consistent with earlier reports for carbonatites from eastern Uganda (Deines and Gold, 1973; Dennis and Schrag, 2010). Although both carbon and oxygen isotope compositions including the published data fall in the mantle field (delimited by Nelson et al., 1988),

Table 1
Chemical composition of carbonatite samples from this study.

	AC01A	AC01C	AC01E	AC01F	AC03B	AC03C
	Carbonatite	Carbonatite	Carbonatite	Carbonatite	Carbonatite	Carbonatite
Major elements (wt%)						
SiO_2	0.78	2.69	10.25	0.27	4.16	12.35
TiO_2	0.02	0.05	0.04	0.03	0.05	0.30
Al_2O_3	0.24	6.39	4.31	0.10	0.19	0.79
Fe_2O_3	<0.01	0.73	<0.01	<0.01	1.97	0.70
FeO	0.53	2.50	2.00	3.30	1.65	3.69
MgO	1.65	3.72	7.73	11.29	0.40	1.47
MnO	0.13	0.15	0.20	0.52	0.21	0.29
CaO	52.99	45.14	38.90	39.26	51.31	48.37
Na_2O	0.10	0.13	0.32	0.07	0.77	1.42
K_2O	0.25	0.35	1.90	0.16	0.06	0.39
P_2O_5	2.52	4.73	4.43	3.25	1.76	3.97
F	0.30	0.35	0.85	0.56	0.32	0.41
CO_2	41.27	33.40	26.95	41.37	37.97	25.35
S	<0.01	0.02	<0.01	<0.01	<0.01	0.02
LOI	<0.05	<0.05	2.29	<0.05	<0.05	<0.05
H_2O	0.15	0.14	0.20	0.07	0.11	0.10
Total	99.74	99.93	99.89	99.53	99.58	99.54
Trace elements (ppm)						
Li	5.74	6.65	4.67	2.16	3.24	9.96
Sc	3.23	8.16	5.08	1.47	bdl	bdl
V	11.3	39.4	15.0	19.6	158	229
Cr	1.20	0.59	4.94	1.94	bdl	bdl
Co	1.23	12.7	5.58	5.97	3.92	9.20
Ni	1.25	0.89	2.16	1.15	0.81	0.41
Cu	bdl	2.13	0.61	bdl	2.70	4.31
Zn	1.99	45.3	49.6	180	17.7	85.4
Ga	2.74	4.81	7.71	3.08	3.41	9.27
Rb	2.74	3.20	21.6	0.40	0.86	4.94
Sr	3571	3094	3261	3211	6586	3854
Y	46.8	40.5	49.6	38.5	24.1	37.5
Nb	5.59	20.0	53.5	346	113	97.9
Zr	11.2	216	7.20	0.12	9.88	99.6
Cd	0.10	0.11	0.16	0.54	0.32	0.24
Cs	0.05	0.09	0.78	0.01	0.01	0.09
Ba	393	375	976	2707	614	607
La	149	160	160	311	133	207
Ce	311	343	343	507	255	461
Pr	34.0	38.7	38.3	59.8	25.4	49.7
Nd	138	158	154	221	90.2	185
Sm	23.4	26.4	26.4	35.6	14.3	28.6
Eu	6.59	7.26	7.28	10.8	4.26	8.23
Gd	20.2	22.2	22.1	28.4	11.5	21.1
Tb	2.47	2.63	2.71	3.91	1.45	2.56
Dy	11.8	12.0	12.9	16.6	6.14	10.4
Ho	1.87	1.88	2.03	3.08	1.16	1.82
Er	4.38	4.24	4.84	5.94	2.47	3.75
Tm	0.47	0.44	0.51	0.65	0.31	0.45
Yb	3.05	2.75	3.41	2.91	1.70	2.39
Lu	0.36	0.32	0.39	0.40	0.26	0.38
Hf	0.28	3.37	0.17	0.03	0.14	1.10
Ta	0.87	3.83	5.64	2.42	1.57	3.32
Tl	0.17	0.07	0.12	0.01	0.05	0.04
Pb	3.25	4.35	3.83	48.2	6.52	7.66
Th	0.64	0.35	2.41	0.08	0.14	28.4
U	0.13	1.75	3.42	7.61	2.80	1.47
ΣREE	707	780	778	1208	547	982
La_N/Yb_N	33.9	40.3	32.5	73.9	54.0	60.0

apparently they form various trends.

4.6. Noble gas isotope systematics

4.6.1. Helium

Noble gas concentrations and isotope ratios are summarized in Table 3. The ^{4}He concentrations in the whole-rock samples containing calcite+apatite+silicate are (1.16–6.90) × 10^{-7} ccSTP/g and (3.79–71.44) × 10^{-7} ccSTP/g in Tororo and Sukulu, respectively. A systematic variation in He concentrations and isotope ratios between the two complexes is not observed. Helium concentrations in apatite from Tororo are comparable with the bulk samples at (4.71–7.57) × 10^{-7} ccSTP/g, whereas pyroxene separates released significantly less ^{4}He (0.38–1,26 × 10^{-7} ccSTP/g) than the corresponding bulk samples.

The R/R_a ratios [where R stands for the measured $^3He/^4He$ ratio and R_a for the atmospheric $^3He/^4He$ ratio (≡1.38 × 10^{-6})] show a systematic variation among the two complexes as well as between the various mineral separates of Tororo samples. The highest values up to 9.3R_a measured on whole rocks were found in the Sukulu complex. Separated calcite samples from Tororo yield similarly high values between 7.19 and 8.82R_a. Compared to calcite, the intermediate values were measured in the bulk rock samples (5.62 and 8.18R_a) and the lowest

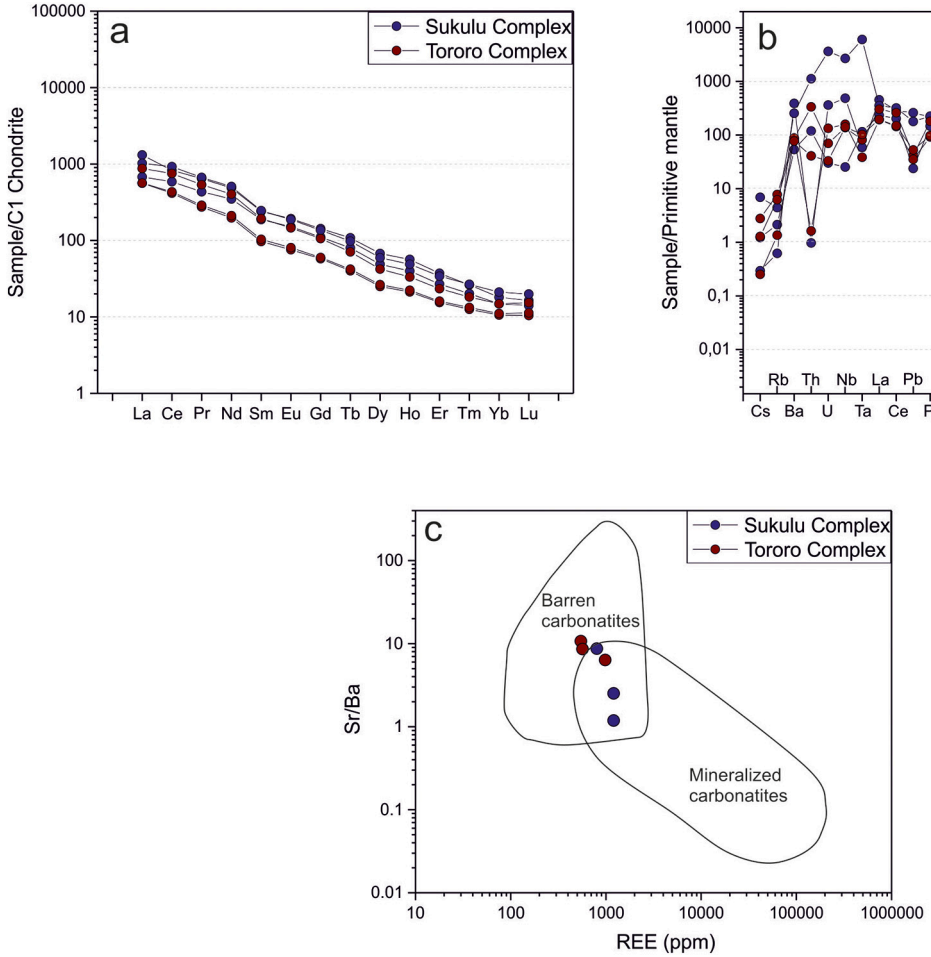

Fig. 7. **a**, CI-chondrite normalized rare earth element concentrations in the two complexes. No steep LREE pattern was found, otherwise characteristic for carbonatites, but in line with other localities the lack of negative Eu anomaly indicates a mantle origin. Chondrite-normalizing values of Anders and Grevesse (1989) were used. **b**, The primitive mantle-normalized trace element plot of carbonatites. Note the pronounced negative Zr-Hf anomaly and Pb depletion for most samples. Normalization values were taken from McDonough and Sun (1995). **c**, A plot of ΣREE vs. Sr/Ba indicates a barren, non-mineralized character of the studied carbonatites (Hou et al., 2015).

values were obtained for pyroxene (4.63–5.28R_a) and apatite (2.21–3.10R_a) fractions. The highest $^3He/^4He$ of 9.3R_a was measured in the olivine-bearing carbonatite AC01C from Sukulu. In contrast, the lowest $^3He/^4He$ of 5.15R_a was found for sample AC01F which is also consistent with secondary mineralogical and textural features (alvikite vein, bastnäsite, barite, sphalerite, galena), as well as slightly different stable C-O isotope systematics.

Stepwise crushing experiments performed on three whole-rock samples (AC01C, AC03B, AC03I) show similar systematics. Compared to the single-step crushing (100 strokes), the two-step crushing (150 strokes) resulted in higher He concentrations. Further, the extended crushing yielded higher $^3He/^4He$ ratios (AC01C: 9.60 vs. 9.05R_a; AC03B: 7.78 vs 7.47R_a; AC03I: 9.35 vs. 8.48R_a). This might indicate a presence of two generations of fluid inclusion which differ in size and, to some extent, He isotope compositions. During the first crushing mainly the larger size inclusion were opened, while during the extended crushing the smaller-size inclusions released their noble gas content with slightly elevated $^3He/^4He$ ratios. Moreover, relatively high R values might indicate a possible contribution from cosmogenic ^3He. Experimental results of Scarsi (2000) proved that limited crushing (few hundred strokes and < 2 min) liberated noble gases exclusively from the fluid inclusions and gentle crushing was verified as the most adequate way to separate pristine and cosmogenic (mineral lattice hosted) noble gas components. The extended crushing in our case can still be regarded as gentle crushing as only 150 strokes were applied. In addition, the studied samples derived from sites, which previously were covered by a thick regolith sheet and, therefore, the amount of cosmogenic ^3He in our samples is very likely insignificant.

4.6.2. Neon

Bulk-rock ^{22}Ne concentrations of samples from Sukulu and Tororo vary between (3.89–11.5) × 10^{-11} ccSTP/g and (4.6–8.8) × 10^{-11} ccSTP/g, respectively (Table 3). The $^{20}Ne/^{22}Ne$ and $^{21}Ne/^{22}Ne$ ratios of bulk-rock samples as well as calcite, pyroxene and apatite separates are plotted in Fig. 10a. All carbonatite samples investigated here differ from the Ne isotope systematics of the atmosphere by more than 1σ uncertainties. Except for the sample AC01E, all data lie on a vector slightly steeper than the air–DMM trend and show mixing between the atmospheric and DMM end members. Following the method of Moreira et al. (1995), each sample was extrapolated through air to a $^{20}Ne/^{22}Ne$ ratio of 12.5 (Neon-B: Holland and Ballentine, 2006; Trieloff et al., 2000) to obtain the extrapolated, air-free $(^{21}Ne/^{22}Ne)_{EX}$ ratio. The extrapolated $^{21}Ne/^{22}Ne$ ratios fall between 0.024 and 0.07. The sample AC01E (Sukulu) showed extremely high $^{20}Ne/^{22}Ne$ (11.84) and low $^{21}Ne/^{22}Ne$ (0.033) ratios plotting close to the Iceland trend (Graham, 2002), indicating a presence of a deep mantle component.

Pyroxene and apatite separates (Fig. 10b) show higher [(9.5–10) × 10^{-11} ccSTP/g)] and lower [(0.9–1.1) × 10^{-11} ccSTP/g)] ^{22}Ne concentrations than calcite and whole-rock samples, respectively. AC03C apatite and AC03B pyroxene have more radiogenic Ne isotope

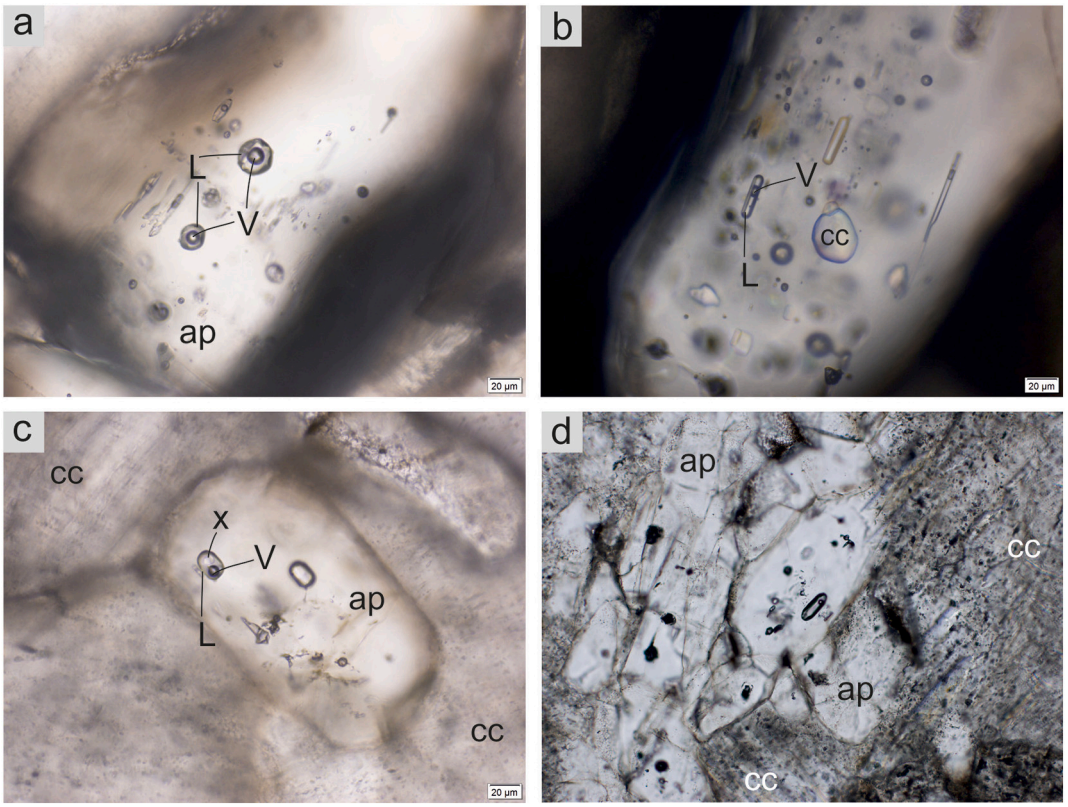

Fig. 8. Fluid inclusion petrography: **a**, Type I two phase liquid–vapor inclusions in the core of an apatite crystal; **b**, Type I two phase liquid–vapor and Type III solid calcite inclusions in the core of an apatite crystal; **c**, Type II three phase liquid–vapor–solid fluid inclusions in the core of an apatite crystal; **d**, a cluster of apatite crystals with primary fluid inclusions.

compositions, with almost crustal $^{20}Ne/^{22}Ne$ ratios (9.48 and 9.73, respectively) indicating that a significant nucleogenic $^{22}Ne^*$ component has been produced via the reaction $^{19}F(\alpha, n)^{22}Na(\beta^+)^{22}Ne$. Contamination of calcite with pyroxene can be excluded, but apatite has not been separated from calcite and, therefore, tiny (fluor)apatite crystals in calcite may shift the $^{20}Ne/^{22}Ne$ ratios towards more nucleogenic values. Stepwise crushing experiments carried out on selected bulk-rock samples (AC01C, AC03B, AC03I) show that Ne isotope ratios after 50 strokes are enriched in nucleogenic $^{22}Ne^*$ and $^{21}Ne^*$ (Table 3). The $^{22}Ne^*$ can be derived from ^{19}F and the reaction $^{24,25}Mg(n,\alpha)^{21,22}Ne$ could also produce nucleogenic $^{21}Ne^*$ and $^{22}Ne^*$. Moroever, due to the very low Mg concentration of the samples, the effect of the latter reaction is assumed to be insignificant. The only reaction that can be considered to produce $^{21}Ne^*$ and $^{20}Ne^*$ is the $^{17,18}O(\alpha,n)^{20,21}Ne$. However, calculating with the-present day crustal production rates (Leya and Wieler, 1999), in the past ca. 40 million years several magnitude less Ne has been produced via these reactions than the measured values. Neon isotope compositions measured in the second step (150 strokes) are more mantle-like. The elevated $^{22}Ne^*$ and $^{21}Ne^*$ concentrations found both in apatite as well as during stepwise crushing indicate that the measured MORB-like $^{20}Ne/^{22}Ne$ and $^{21}Ne/^{22}Ne$ ratios in the bulk-rock samples have to be taken as minimum estimates for the mantle source compositions.

Whereas the Ne isotope ratios show the same trend for both suites, there is a significant difference in the extent of atmospheric contaminations. Both the simple and the extended crushing show that the Tororo samples are more enriched in the atmospheric component compared with Sukulu carbonatites (with a maximum cut-off upper limit in $^{20}Ne/^{22}Ne$ ratios of ~10.35; Fig. 10c). Such dissimilarity well corresponds to distinct radiogenic Sr-Nd isotopic signature associated with different associations of silicate minerals as observed by Ackerman et al. (2021). These authors explain more radiogenic character of aegirine-bearing Tororo carbonatites in terms of slower ascent to the surface, resulting in fractionation of K-Mg phases (phlogopite and olivine) and low-degree assimilation of albite-rich country rocks. Alternatively, this difference might have been due to the admixture of magma/hydrothermal fluids during crystallization or interaction with hydrothermal fluids of meteoric origin.

4.6.3. Argon

The ^{40}Ar concentrations in the whole-rock samples, consisting dominantly of calcite, range (1.53–12.63) $\times$ 10^{-7} ccSTP/g, and the observed $^{40}Ar/^{36}Ar$ ratios vary from 305 to 906; $^{40}Ar/^{36}Ar > 1000$ was only found in sample AC01E from Sukulu, which also showed significantly higher $^{20}Ne/^{22}Ne$ (11.84) compared to the other samples. The air-like (295.5; Lee et al., 2006) $^{40}Ar/^{36}Ar$ ratios are in line with low K contents of the samples ($K_2O < 0.4$ wt%) and, therefore, the measured Ar isotope ratios most probably reflect the mixture of the air and minor mantle components. The sole exception of sample AC01E ($^{40}Ar/^{36}Ar =$ 1352) indicates minor phlogopite impurity in the analyzed sample.

5. Discussion

5.1. Magmatic and hydrothermal processes inferred from mineral textures and mineral chemistry

In order to understand various isotope fingerprints and distinguish between shallow level crustal versus deep mantle processes it is essential to reconstruct the magmatic–hydrothermal evolution of the carbonatites based on rock petrography and mineral chemistry. In the Sukulu complex the main silicate mineral phases are olivine and phlogopite. Whereas olivine is a truly magmatic mineral, phlogopite is a common mineral in primary carbonatites but also in fenites. Primary magmatic pyroxene in most nephelinites, ijolites and similar alkaline silicate lithologies, associated with carbonatites, is augite or aegirine-augite.

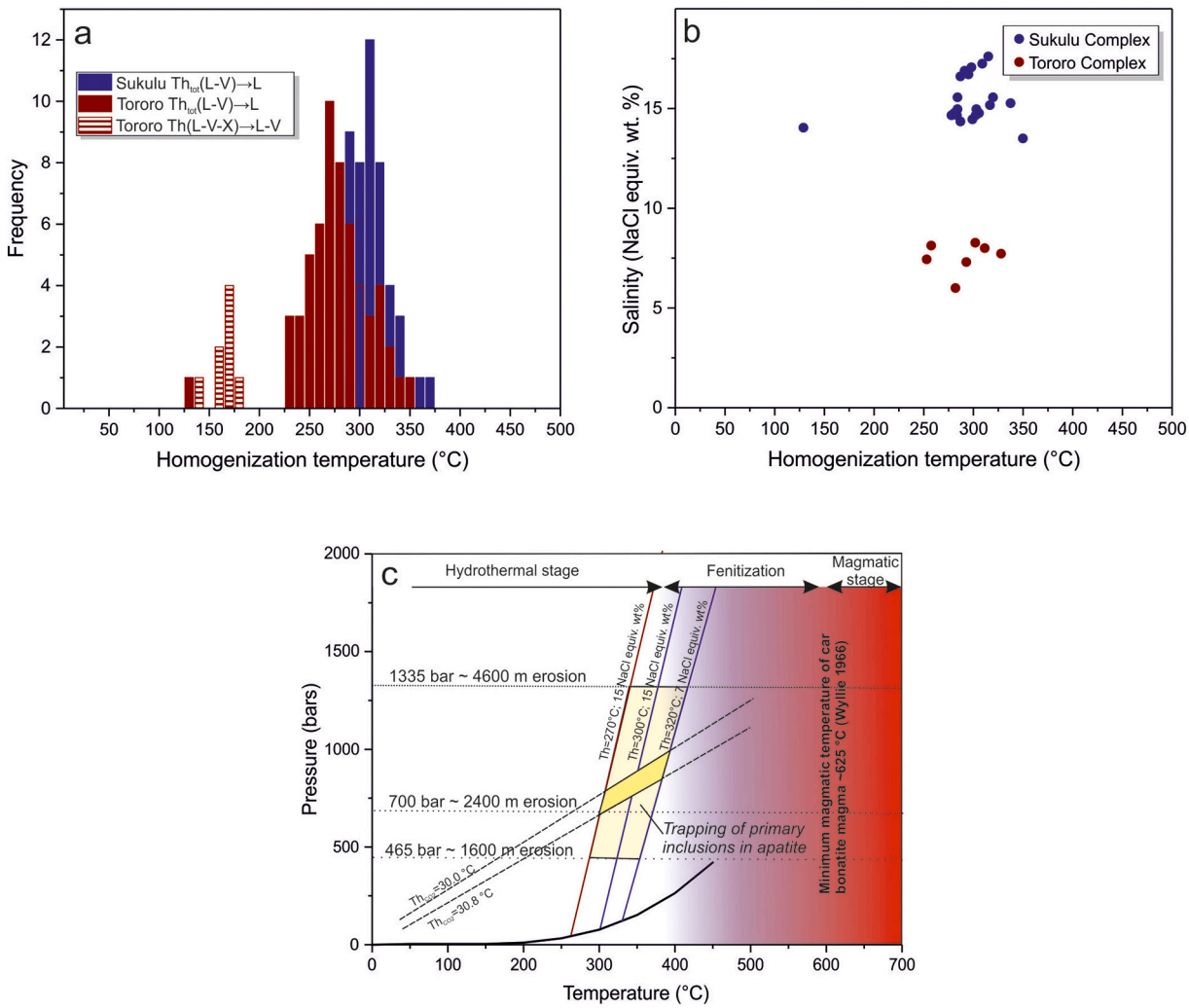

Fig. 9. Results of fluid inclusion microthermometry. **a**, The homogenization temperature distribution diagram (L–liquid, V–vapor, X–solid phase, probably nahcolite). **b**, The homogenization temperature vs. salinity diagram of fluid inclusions. **c**, The pressure correction for aqueous liquid–vapor inclusions calculated from the estimated erosional depth. The yellow field indicates the probable trapping conditions of the primary aqueous inclusions. The 465–700 bar range represents the most probable depth/pressure range implying the formation of apatite at a relatively shallow depth, under hydrothermal conditions. For reference the theoretical isochores of pure CO_2 inclusions with homogenization temperatures of almost 30.0 °C and 30.9 °C were also plotted. Assuming unmixing between the aqueous and carbonic phase, the intercept of the isochores defines the field of the trapping temperature and pressure. The calculated field perfectly overlaps with the field derived from erosional rates. (For interpretation of the references to colour in this figure legend, the reader is referred to the web version of this article.)

Aegirine, found as a ubiquitous phenocryst phase present in all samples from Tororo, has mainly been reported from autometasomatically (internally altered) fenitized alkaline rocks (e.g., Ilímaussaq, Greenland – Markl and Baumgartner, 2002; Montviel, Canada – Nadeau et al., 2016) or in real fenites such as Alnö, Sweden (Morogan and Martin, 1985) or Fen, Norway (Kresten and Morogan, 1986), but it has been found as an orthomagmatic phase as well (Siriwasan: Viladkar and Gittins, 2016). The chemistry of pyrochlore found as inclusions in some aegirine crystals may attest to the intrinsic origin of aegirine because a clear distinction can be made between magmatic and hydrothermal pyrochlore based on the major element chemistry (Magna et al., 2020; Zurevinski and Mitchell, 2004). The Na- and F-enriched character of pyrochlore in carbonatites from this study clearly points to its magmatic origin and may also provide evidence for the magmatic origin of the host pyroxene. In contrast, the parallel vein-like microstructures in the sample AC01E rather suggest their crystallization from an alkaline-rich fluid. Besides, the occurrence of K-feldspar on the rims of aegirine is a characteristic feature observed in fenites (Elliott et al., 2018) and points to the incipient autometasomatic fenitization of carbonatite. Moreover, pyrite has partly been altered to siderite. Because both K-feldspar and siderite are embedded in aegirine a post-magmatic hydrothermal overprint must have modified the primary magmatic mineral assemblage.

Crystal morphology as well as variations in trace element contents between the rims and cores of apatite have been found useful in discriminating among (sub)volcanic, plutonic and hydrothermal apatite in carbonatitic rocks (Chakhmouradian et al., 2017). The pillow-like shape, a prismatic habit commonly with embayed contours of the apatite, as a well as their common intergrowths with euhedral phlogopite in the Sukulu complex would indicate a plutonic origin for most of the mineral phases. Inclusion-free rims and Sr enrichment of apatite have been observed in many magmatic (e.g., Fen: Andersen, 1986; Jacupiranga, Brazil: Costanzo et al., 2006) and hydrothermally overprinted (Tundulu, Malawi and Kangankunde, Mozambique: Broom-Fendley et al., 2016) carbonatite complexes. Because Sr tends to concentrate with decreasing temperature at subsolidus conditions in hydrothermal phases (e.g., barite, strontianite), the external Sr-rich zone might also have crystallized at a subsolidus temperature. Apatite with inclusion free-rims as well as the elevated Sr concentrations in the rims of apatite suggest that the rims of the crystals and some individual crystals have grown from a hydrothermal fluid at subsolidus

Table 2
Stable carbon and oxygen isotope data for carbonatites from this study.

	Lithology	$\delta^{13}C_{V\text{-}PDB}$ (‰)	$\delta^{18}O_{V\text{-}SMOW}$ (‰)	Laboratory
Sukulu				
AC01A	Carbonatite	−3.27	7.39	CGS
		−3.32	7.48	INR
AC01C	Carbonatite	−3.35	7.57	CGS
	Replicate	−3.34	7.58	CGS
		−3.36	7.59	INR
AC01E	Carbonatite	−3.42	8.16	CGS
		−3.33	8.12	INR
AC01F	carbonatite	−1.07	8.88	CGS
		−0.90	9.49	INR
Tororo				
AC03B	Carbonatite	−3.61	7.94	CGS
		−3.71	8.06	INR
AC03C	Carbonatite	−3.70	7.83	CGS
		−3.76	8.07	INR
AC03I	Carbonatite	−3.85	7.76	INR
Reference materials				
NBS-18 (IAEA)		−4.99	7.20	CGS
JLs-1 (GSJ)		2.02	26.19	CGS

CGS – Czech Geological Survey, Prague, Czech Republic; INR – Inst. Nuclear Research, Debrecen, Hungary.
Replicate analysis of sample AC01C involved a full analytical protocol and measurement procedure. Standard deviation is ±0.08‰ for $\delta^{13}C$ and ±0.1‰ for $\delta^{18}O$ measurements at INR.

temperatures. Moreover, apatite with fluid inclusion-rich cores always occurs in the inter-crystalline space, and the calcite solid inclusions of Type III found in apatite indicate the following crystallization sequence: pyrochlore/olivine/aegirine → calcite + apatite→ apatite + phlogopite. Considering the eutectic temperature of the carbonate liquid at 610–625 °C (Jones and Wyllie, 1986; Wyllie, 1966), apatite must have crystallized at these temperatures or below.

Corrosion of olivine, chloritic alteration of phlogopite, sieve-textured dolomite as well as the occurrence of hydrothermal mineral phases (pyrite rimmed by siderite, galena, barite, bastnäsite) further attest to a hydrothermal overprint of the primary mineral assemblage. According to experimental studies and observations on melt inclusions (Green and Wallace, 1988; Guzmics et al., 2008; Guzmics et al., 2011; Lee and Wyllie, 1998; Sweeney, 1994), dolomitic magmas originate directly from the mantle, whereas calcio-carbonatites undergo significant fractionation and immiscibility during their ascent. Given that the studied carbonatite is a calcio-carbonatite, magmatic origin of the dolomite is less likely and favors a hydrothermal origin.

The C-O isotope data also support hydrothermal influence because even though they plot in the field of primary carbonatites of Nelson et al. (1988) or close to the field determined by Taylor et al. (1967). When combined with available data for Uganda from literature (Deines and Gold, 1973; Dennis and Schrag, 2010) they form a broadly positive trend. This positive trend can be explained by 1) liquid immiscibility of carbonate – silicate, 2) fractional crystallization (e.g. Deines, 1989; Demény et al., 1998; Ray et al., 2000), 3) assimilation of crustal material (e.g., Demény and Harangi, 1996; Hoernle et al., 2002), or 4) hydrothermal processes: fluid–rock interactions (Comin-Chiaramonti et al., 2005; Deines, 1989). The petrographic observations (see above) and fluid inclusion microthermometry (e.g., homogenization temperature and the inferred trapping temperature; see next section) indicate hydrothermal processes, therefore this explanation is favored here to explain the observed C-O isotope systematics.

In addition, a shift towards more positive $\delta^{13}C$ values (without a concomitant change of $\delta^{18}O$) is also observed in Fig. 11. It should be noted though that from the current sample suite only sample AC01F is characterized by this feature. This shift might indicate that some small scale crustal assimilation took place during the magma ascent or the magma source has been affected by recycled carbon (e.g., Lustrino et al., 2020). Although the $^3He/^4He$ ratio of this sample is lower (5.16 R_a) than found for the other samples, it should be emphasized that the He isotope signal might, in part, be affected by noble gases derived from apatite as a whole rock was analyzed. Nevertheless, the majority of the samples do

Table 3
Noble gas elemental and isotope compositions of whole-rock and mineral fractions of carbonatites from this study.

	Phase	Number of strokes	Sample weight (g)	^4He [$\times10^{-7}$ ccSTP]	R/R_a	^{22}Ne [$\times10^{-11}$ ccSTP]	$^{20}Ne/^{22}Ne$	$^{21}Ne/^{22}Ne$	^{40}Ar [$\times10^{-7}$ ccSTP]	$^{40}Ar/^{36}Ar$
Sukulu										
AC01A	WR	100	1.15	3.26	6.51	3.89	10.44	0.036	2.20	503.7
AC01C	WR	100	1.03	5.35	8.87	4.39	10.85	0.036	2.58	467.1
	WR 1st step	50	1.16	3.71	9.05	2.75	10.69	0.038	2.43	446.5
	WR 2nd step	100	1.16	3.19	9.60	1.84	11.10	0.041	2.09	459.1
	WR 1st + 2nd step	150	1.16	6.90	9.30	4.59	10.85	0.039	4.52	452.2
AC01E	WR	100	1.31	2.49	8.88	5.86	11.84	0.033	12.63	1352.1
AC01F	WR	100	1.99	2.58	5.15	11.46	10.32	0.034	11.20	906.2
Tororo										
AC03B	WR	100	1.91	4.60	6.60	8.79	9.87	0.028	6.84	378.2
	Apatite	100	1.59	7.57	3.10	1.12	10.25	0.034	0.80	546.4
	Pyroxene	100	1.01	0.38	4.63	9.55	9.73	0.032	1.68	305.4
	Calcite	100	1.55	5.51	8.16	2.56	10.92	0.027	2.52	483.5
	WR 1st step	50	1.05	4.95	7.47	3.21	9.59	0.033	0.87	378.2
	WR 2nd step	100	1.05	4.68	7.78	1.39	8.87	0.029	0.67	372.3
	WR 1st + 2nd step	150	1.05	9.63	7.62	4.60	9.38	0.032	1.53	375.6
AC03C	WR	100	1.55	3.79	5.62	6.42	10.02	0.030	6.59	365.8
	Calcite	100	1.49	8.68	7.19	3.37	10.35	0.031	3.51	531.7
	Apatite	100	1.60	4.71	2.21	0.90	9.48	0.034	0.49	389.7
AC03I	Calcite	100	1.03	85.40	8.82	8.33	9.98	0.032	1.29	483.3
	WR 1st step	50	0.92	28.69	8.48	3.84	9.75	0.033	1.02	412.7
	WR 2nd step	100	0.92	42.75	9.35	4.08	9.97	0.032	3.73	593.2
	WR 1st + 2nd step	150	0.92	71.44	9.00	7.93	9.86	0.032	4.75	542.3
	Pyroxene	100	1.03	1.26	5.28	10.02	9.97	0.030	7.29	305.6

Errors in the noble gas compositions are ±3%. Errors in isotopic values are at the 1σ level.
WR – whole-rock.

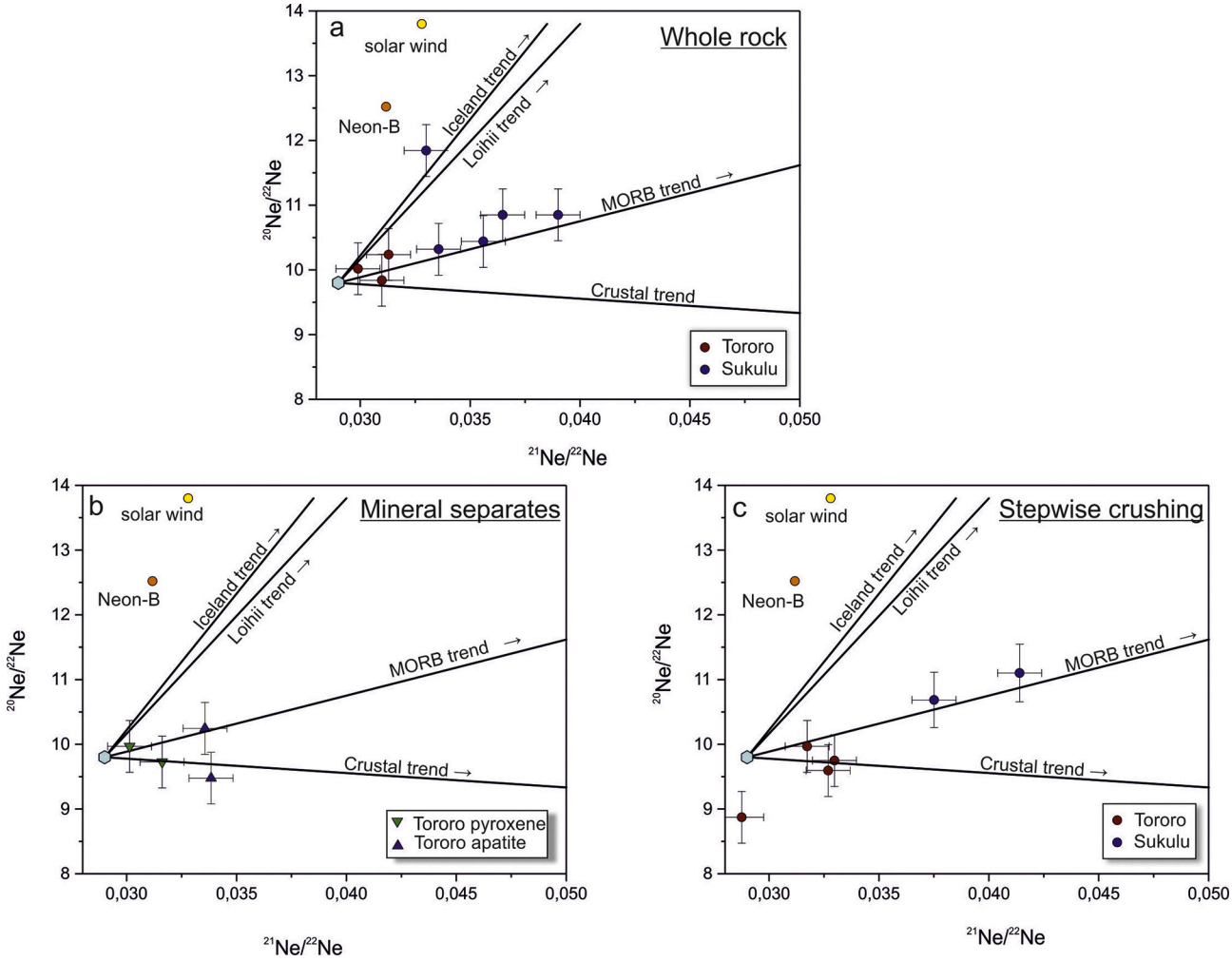

Fig. 10. Neon three-isotope plot of carbonatites from Tororo and Sukulu. **a**, Whole-rock samples. **b**, Mineral separates. **c**, Stepwise crushing. Trendlines towards the continental crust (Kennedy et al., 1990); oceanic island basalts (Loihi, Hawaii: Valbracht et al., 1997); Iceland: (Trieloff et al., 2000) have been plotted for reference. Yellow circle indicates the solar wind composition, the orange circle represents the Neon-B Ne isotope ratios (Trieloff et al., 2000; Trieloff and Kunz, 2005). Uncertainities given correspond to 1σ. (For interpretation of the references to colour in this figure legend, the reader is referred to the web version of this article.)

not show this systematics having high $^{3}He/^{4}He$ ratios; therefore, we argue that if some crustal assimilation took place, it was limited and it took place during the magma ascent rather than in the mantle. In the Fig. 11 the isotopic compositions of Fort Portal carbonatites (Deines and Gold, 1973), which represent different settings within EAR, are also plotted. The observed isotopic systematics might indicate surficial processes like degassing and weathering (e.g., Demény and Harangi, 1996; Demény et al., 2004).

5.2. *Fluid inclusions: magmatic or hydrothermal origin?*

Pressure and temperature conditions of entrapment as well as the chemical nature of fluid and solid inclusions hosted by apatite in Sukulu and Tororo have been discussed elsewhere (Rankin, 1977; Ting et al., 1994a, 1994b). Ting et al. (1994a) distinguished three fluid inclusion assemblages: (1) a CO_2–H_2O–NaCl dominant, (2) a H_2O–NaCl dominant, and (3) a CH_4-bearing assemblage in drill cores of the Sukulu complex from the depths of up to 118 m. They concluded that the fluids evolved chemically from an Mg-bearing calcite melt through aqueous CO_2-bearing and bicarbonate-rich melts. Methane-bearing fluid inclusions were only found in one drill core sample and were interpreted as the final, late hydrothermal fluids.

In the samples, two-phase aqueous–vapor inclusions apparently coexist with multi-solid phase inclusions. Nahcolite dissolved at around 170 ± 20 °C into a liquid phase indicates that it is a daughter product of an alkaline-rich aqueous liquid. Nahcolite is a common solid phase identified in many carbonatite complexes (Andersen, 1986; Guzmics et al., 2011; Rankin and Le Bas, 1974; Roedder, 1984) and fenites, and suggests the presence of alkaline carbonate fluids during apatite crystallization. Guzmics et al. (2019) posit that alkaline carbonate fluids of the Pleistocene Kerimasi volcano (Tanzania) may play a significant role during the formation of natro-carbonatites through mixing of F-rich carbonate melt and alkaline carbonate liquids. Alternatively, de Moor et al. (2013) suggested that natro-carbonatite at Oldoinyo Lengai (Tanzania) formed by outgassing of a hydrous carbonate fluid coexisting with a nephelinite melt which may have subsequently unmixed to produce "wet" vapor and natro-carbonatitic liquid. Both processes producing alkali carbonate liquids involve the presence of alkaline-rich carbonate fluids that may precipitate nahcolite at subsolidus temperatures. The alkali carbonate rocks are, however, prone to rapid alteration and are easily replaced by secondary calcite (Chen et al., 2013). Alkalies (Na, K) and other trace elements (halogenides, REE) that are dissolved from primary alkali carbonate minerals are transported hydrothermally and may result in fenitization of the host carbonatite or the hanging wall-rock lithology. Whereas the alkaline carbonatite rock is not preserved in the geologic record, nahcolite and other alkaline carbonates in the fluid inclusions of Tororo and Sukulu provide a strong support for the presence of alkaline-rich fluids of magmatic origin during the late

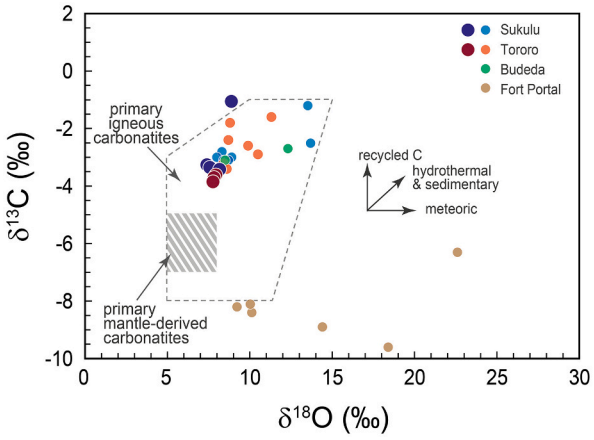

Fig. 11. The $\delta^{13}C$ and $\delta^{18}O$ values of calcite from carbonatites of the Sukulu and Tororo complexes. The gray box indicates the characteristic mantle values by Nelson et al. (1988) and the dashed box is for primary igneous carbonatites (Ray and Ramesh, 2006). Stable C-O isotope values of published samples from the Tororo, Sukulu, Bukusu and Fort Portal carbonatites (Deines and Gold, 1973; Dennis and Schrag, 2010) have also been plotted. (For interpretation of the references to colour in this figure legend, the reader is referred to the web version of this article.)

stages, at the magmatic–hydrothermal transition. Nevertheless, CO_2- and CH_4-rich inclusions were not identified in the new samples from Sukulu although both gases have been found in trace amounts in the gas phase of the H_2O–NaCl inclusions, which is common in fenitic fluids (Elliott et al., 2018).

Pressure and temperature conditions of trapping are difficult to estimate as no phase diagrams of the H_2O + NaCl+$NaHCO_3$ system have yet been reported. Isochores for other nahcolite-bearing fluids in carbonatites or metamorphic rocks were constructed using the NaCl+H_2O binary system (Liu and Fleet, 2009) and employing the equation of state by Bowers and Helgeson (1983). Following this practice, the fluids were modeled with the NaCl + H_2O binary system and the isochores were constructed using the equation of state reported by Bodnar and Vityk (1994; Fig. 9c). Due to the uniform liquid-to-vapor ratios, i.e. homogeneous trapping, the isochores provide only the minimum trapping temperature and pressure. In order to estimate the real trapping pressure and temperature conditions, a pressure correction has to be performed using either an independent thermometer or barometer. As it has been demonstrated, apatite crystallized at or below 625 °C. Because it is intergrown probably with fenitic phases, the crystallization temperature can be extended down to the minimum temperature of fenitization. For the minimum temperature limit of fenitization 500 ± 30 °C at 1 kbar has been used, defined by the stability of the aegirine–augite–microcline–perthite paragenesis (Elliott et al., 2018, and references therein). Intersecting the isochores (T_h = 300 °C and 15 NaCl equiv. wt%) with the 500 °C and 625 °C isotherms, the calculated pressures are 2575 and 4321 bars, respectively, that correspond to the respective depths of ~8.9 km and 14.9 km under lithostatic conditions. Ting et al. (1994a) and others (e.g., Fen Complex: Andersen, 1986) used the carbonatite solidus of Wyllie (1966) at 625 °C for pressure correction and reported higher pressures, even up to 6 kbar that would correspond to 19–20 km depth. They argued that crystallization of the host apatite in carbonatite liquids is stable over a wide temperature range (Biggar, 1967) and that apatite crystallizes at mid-crustal levels prior to calcite crystallization, and is then transported with the magma to the shallow crust. However, in Sukulu and Tororo apatite occurs in the form of intercrystalline phase between calcite crystals and not as inclusions directly embedded in calcite. Therefore, the model invoking the crystallization of apatite at mid-crustal levels at high pressures is not favored.

Instead, the calculated average incision rates (AIR) have been applied as an independent barometer for pressure correction. According to Xue et al. (2019) the AIR in the Kenya Rift varied between 1 and 275 mm/kyr since the Pliocene (4.5 Ma) whereas prior to the Pliocene it did not exceed 50 mm/kyr. Considering the Oligocene age (28 Ma) of the carbonatites and taking into account the maximum AIR values, the total estimated erosional depth is 2412 m. With a more realistic calculation, assuming 150 mm/kyr and 30 mm/kyr before and after 4.5 Ma (Elliott et al., 2018), the estimated erosion is 1605 m corresponding to 465 bars. Roller et al. (2012) estimated a maximum 4600 m (~1.4 kbar) erosion in the EARS based on the measured uplift rate of 131 mm/kyr. By employing various end-members (Fig. 9c), the real trapping pressures and temperatures could have been between 330 and 425 °C and 465–1330 bars, respectively. In the Tororo complex, apatite formation continued to lower temperatures (ca. 300 °C) from more dense fluids during a subsequent hydrothermal circulation, as evidenced by the low homogenization temperature of 270 °C indicated for Type II fluid inclusions.

5.3. Critical reevaluation of previous fluid inclusion data

The above discussed pressure–temperature estimation is in line with the calculations of Rankin (1977) who first suggested the 'carbohydrothermal' origin of the Tororo carbonatite. It is plausible that unrealistic trapping pressures measured for Sukulu (Ting et al., 1994a) and other carbonatite complexes (e.g., 4–5 kbar estimated for the Fen carbonatite complex, Andersen, 1986; 3–5 kbar for the Siilinjarvi carbonatite complex, Poutiainen, 1995) have been overestimated due to inadequate petrographic observations and the underestimation of the significance of the continuous magmatic–hydrothermal transition or hydrothermal remobilization.

Ting et al. (1994a) reported on the coexisting CO_2- and H_2O-bearing inclusions in the cores of apatite crystals in a single assemblage from Sukulu, but interpreted them separately. They proposed that the first generation was a CO_2-rich fluid that evolved into H_2O-dominated fluids and that the pressure decreased from 9 to 3 kbar. However, if the two types of fluid inclusions coexist they can form an immiscible H_2O–CO_2 system and a reliable pressure calculation can be performed by intersecting the isochores of the CO_2-rich and the H_2O-rich end members. In samples from this study no CO_2-rich inclusions were detected but using the homogenization data of Ting et al. (1994a): Th_{CO2} = 30.0–30.8 °C and intersecting them with the 260 °C and 330 °C isochores of the H_2O-bearing inclusions, the obtained pressures (400–1000 bar) overlap with the pressures calculated from the erosion rates. These new calculations further support the earlier assertions of Poutiainen (1995) who reported on the apatite crystallization temperatures of 300 to 420 °C, which was in conflict with the fluid inclusion trapping temperatures in the Siilinjärvi carbonatite complex. While Poutiainen (1995) interpreted the inconsistent data by wide formation temperatures of apatite, our results show that apatite probably formed at much lower temperatures and pressures under hydrothermal conditions than assumed for Siilinjarvi and other carbonatite bodies.

5.4. Considerations of noble gas systematics in EARS carbonatites

5.4.1. Interpretation of noble gas compositions in apatite, pyroxene, bulk samples and step crushing

Obtaining reliable noble gas data from fluid inclusions is less complicated for young and U–Th–K-poor rocks (Kendrick and Burnard, 2013). In contrast, the production of ^4He, ^{21}Ne and ^{40}Ar in a neutron-rich media (high U, Th or K concentration) or in old rocks can significantly shift the corresponding isotope ratios. In the studied samples the U + Th concentrations vary between 0.76 and 29.9 ppm which, coupled with the Oligocene age of the carbonatites, has a significant effect on the observed ratios. Among the studied samples the bulk-rock AC03C aliquot with [U + Th] = 29.9 ppm yielded the lowest $^3He/^4He$ ratio of $5.6R_a$, whereas the bulk-rock aliquot of AC03B with 2.94 ppm U + Th

returned the highest $^{3}He/^{4}He$ of 9.3R_a. Low $^{3}He/^{4}He$ ratios of 2.2–3.1R_a as well as high $^{21}Ne/^{22}Ne$ ratios of apatite and $^{3}He/^{4}He$ ratios of pyroxene separates at 4.6–5.3R_a prove that the U and Th budget of the carbonatite is mainly hosted by pyrochlore, apatite and pyroxene. The highest He isotope compositions obtained in calcite separates (>8R_a) imply that calcite is depleted in U and Th compared to apatite and pyroxene. Consequently, for genetic interpretations the best estimates are the calcite separates. However, the difference between whole-rock and calcite $^{3}He/^{4}He$ ratios is rather low (~0.3R_a) due to the low modal abundance of apatite and pyroxene in the samples. Therefore, He isotope ratios measured on bulk samples can be reliably used for the interpretation.

5.4.2. $^{4}He/^{3}He$–$^{21}Ne/^{22}Ne$ systematics of Tororo and Sukulu carbonatites and the origin of fluids in the EARS

The He–Ne–Ar isotope systematics of mantle xenoliths, basaltic lavas and volcanic glasses of the entire EARS have been extensively studied by Halldõrsson et al. (2014) who pointed out that magmas have a common, deeply rooted mantle source that later mixed with SCLM and/or with DMM. Carbonatites in southeastern Uganda represent in their current position the most distal and one of the earliest products of the same African super-plume (Bell and Simonetti, 2010; Ernst and Bell, 2010) and may thus provide a unique look into the variation of mantle processes of the Kenya Dome, beneath the South Kenyan Rift (Fig. 1). Halldõrsson et al. (2014) showed that solely the He isotope ratios are inadequate to distinguish between various mantle end-members; the measured $^{3}He/^{4}He$ ratios around 8 ± 1 R_a, also characteristic of global MORB (though with some regional variations; Graham, 2002), represent only one of the end-members of the parent magmas. Therefore, the combined He-Ne isotope approach of Halldõrsson et al. (2014) should be followed in order to resolve different end members and establish the source region of the Sukulu and Tororo fluids.

5.4.3. Origin of fluids in the EARS

It is apparent that He isotope ratios of Tororo and Sukulu carbonatite samples with the least contribution from K, U and Th decay point to a DMM source (= 8 ± 1R_a; Graham, 2002) of the mineralizing fluids (Fig. 12). However, considering the contribution of radiogenic ^{4}He and ^{20}Ne derived from apatite, the $^{3}He/^{4}He$ ratios are higher than 9R_a. More crustal-like He isotope ratios measured in apatite may have two reasons: (a) fluid inclusions accumulated radiogenic ^{4}He derived from the host apatite, or (b) during the low-temperature carbohydrothermal evolution of the carbonatite, crustal-derived fluids mixed with primary magmatic fluids. Meanwhile the transport of noble gases during the inclusion–crystal contact is not favored in olivine and pyroxene (Trull and Kurz, 1993) and, hence, probably in calcite neither. The second scenario is further attested by petrographic observations and $^{3}He/^{4}He$ ratios showing the highest R/R_a values in the least altered samples. As a consequence, to evaluate the origin of the primary magmatic fluids (lower mantle plume/DMM/SCLM) samples with the highest $^{3}He/^{4}He$ ratios were selected.

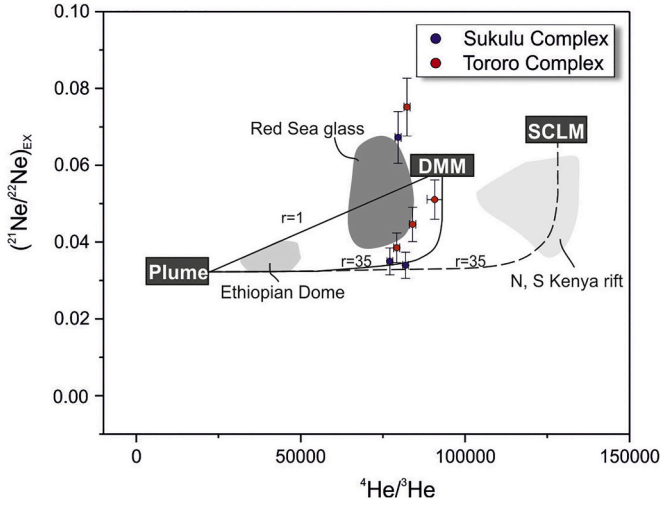

Fig. 12. Extrapolated Ne isotope ratios $(^{21}Ne/^{22}Ne)_{EX}$ versus $^{4}He/^{3}He$ for Sukulu and Tororo. Only the least altered samples AC01C (Sukulu) and AC03I (Tororo) were selected for plotting. Neon isotope ratios are extrapolated to Neon-B ($^{20}Ne/^{22}Ne$ = 12.5; Holland and Ballentine, 2006; Trieloff et al., 2000). For reference, "r" values and the fields of isotope signals (gray colors) of other magmatic rocks from the EARS are also plotted (Halldõrsson et al., 2014). DMM – depleted mid-ocean ridge mantle; SCLM – subcontinental lithospheric mantle.

The Ne isotope data of whole-rock samples also follow the DMM trend defined by the air (Fig. 10a, $^{21}Ne/^{22}Ne$ = 0.029 and $^{20}Ne/^{22}Ne$ = 9.8; Valkiers et al., 1994) and the DMM end-member ($^{21}Ne/^{22}Ne \geq$ 0.0595 and $^{20}Ne/^{22}Ne \geq$ 12.5; Moreira et al., 1995; Holland and Ballentine, 2006; Trieloff et al., 2000), but are always plotting slightly above the air–DMM line. By decoupling the three end members, the air-free $(^{21}Ne/^{22}Ne)_{EX}$ value can be calculated by extrapolating the measured values from the air to a Neon-B end member of $^{20}Ne/^{22}Ne$ = 12.5. By plotting the $^{21}Ne/^{22}Ne_{EX}$ against the $^{3}He/^{4}He$ ratio (Fig. 12) all samples fall on mixing trajectories between PLUME and DMM having $R_a \gg 1$ (see Halldõrsson et al., 2014). Other alkaline complexes, flood basalts and xenoliths from EARS (Halldõrsson et al., 2014 and references therein) show characteristically lower $^{4}He/^{3}He$ ratios (6–8 R_a) and an obvious SCLM component. The single worldwide active carbonatite volcano at Oldoinyo Lengai in the EARS is also characterized by lower $^{3}He/^{4}He$ at ~6 ± 1R_a and the mantle source has been identified as SCLM, that was metasomatized by magmas or fluids from the depleted asthenosphere (Mollex et al., 2018). Exceptions are the volcanic glass samples from the Red Sea, the Afar region, with 8–13.4 R_a and the Rungwe Volcanic Province with $^{3}He/^{4}He$ ratios up to 15 R_a (Hilton et al., 2011; Halldõrsson et al., 2014).

The observed difference between the studied carbonatites compared to other younger and more axially positioned magmatic rocks in the EARS can be explained by the following alternative models: Bell and Simonetti (2010) and Ernst and Bell (2010) argued that the lack of association of basalts to carbonatite magmas in the peripheral zones of the rift is due to the overthickened crust and the plume head that did not reach a sufficiently shallow level to produce voluminous basaltic liquids through plume–lithosphere interaction. If the lithosphere–plume interaction was insufficient, then the peripheral magma had to ascend along deep weakened zones in the mantle and the crust, preserving the isotope signatures of the plume and the DMM. By definition, carbonatite magmas, owing to their low viscosity, ascend rapidly from the mantle with limited interaction with the SCLM.

According to an alternative model, the position (relative distance) of the studied carbonatites with respect to the rift axis during the Paleogene is unclear and may be less significant. Several lines of evidence, such as noble gas (Halldõrsson et al., 2014; Hilton et al., 2011; Hopp et al., 2004), geochronological (George et al., 1998) and radiogenic Sr–Nd–Pb isotope systematics (Furman, 2007; Rogers, 2006) have shown that a uniform magma superplume (African Superplume) exists under the EARS, with one or two heads, that are the centers of deep, mantle-derived magma upwellings (Hilton et al., 2011). Recently, these centers are the Rungwe Volcanic Province in Southern Tanzania and the Afar Region in Ethiopia. During the Paleogene, the studied carbonatites were located ca. 1000 km south from their current geographical position (Fig. 1a). The northern shift of the African continent has displaced the carbonatites which formed above the mantle plume head currently feeding the Rungwe Volcanic Province with plume-derived magmas. This model, assuming a permanent and stable deep-rooted magma source would, however, require a magmatic belt connecting the Rungwe Volcanic Province and southeastern Uganda with gradually younger volcanic rocks and intrusions.

5.4.4. Implications for a possible economic potential

The prerequisites of the formation of large-scale precious/strategic metal or mineral accumulations associated to carbonatites are: (i) the enrichment of the parent carbonatite liquid through element remobilization from a subducting oceanic plate (e.g., giant REE-deposits in China; Hou et al., 2015), (ii) magma–footwall interaction, i.e. fenitization by carbothermal fluids (e.g., Fen carbonatite: Kresten and Morogan, 1986; Amba Dongar: Magna et al., 2020), and (iii) hydrothermal remobilization of apatite (Broom-Fendley et al., 2016). Given that the carbonatite crystallized at a relatively great depth and the complex in its current form represents a deeply eroded part of an alkali intrusion, the shallow level-extended interaction between crustal fluids and the carbonatite magma was inhibited. This is also supported by the stable isotope compositions and the noble gas isotope ratios of the entrapped fluids. Noble gas isotope analysis confirms a plume component in the parent magma with little or no contribution from a subducting lithosphere or the SCLM. This is further advocated by the the Sr/Ba vs. ΣREE plots (Fig. 4c) implying no fluid-related enrichment and ratios characteristic for barren carbonatites worldwide.

Solely the low temperature hydrothermal (re)mobilization in the waning stage of the carbohydrothermal process can be a candidate for precious/strategic element accumulation. In some samples the anomalously high P_2O_5 contents (3–6 wt%) are in line with the observed high modal proportion of apatite and support anomalous apatite concentration that might be the reason for apatite accumulation in the residual soils in the Sukulu hills. A high apatite modal abundance is, however, not accompanied by REE, Sc, V or Zr accumulation and the REE patterns of the carbonatites are similar to other carbonatites worldwide (Jones et al., 2013).

6. Conclusions

Combined petrographic, fluid inclusion and light noble gas investigation of two calcio-carbonatite bodies of Sukulu and Tororo, Uganda, in an off-axis position of the East African rift valley revealed that:

(i) Except for a few olivine-bearing samples most of the carbonatites show mineralogical and textural evidence of fenitization and hydrothermal alteration, which probably significantly influenced the primary mantle plume- and DMM-like isotope signatures.

(ii) Primary aqueous fluid inclusions in the cores of inter-cumulus apatite prove their formation at relatively shallow depths and pressures (465–1335 bar). The alkaline aqueous, dominantly primary magmatic fluids prove a continuous transition from fenitization towards low-temperature hydrothermal processes and probably remobilization.

(iii) Revision of previous fluid inclusions studies of Sukulu and Tororo complexes and other calcio-carbonatite occurrences suggests that unmixing of aqueous–carbonic fluids trapped simultaneously attests to a late-hydrothermal origin of the fluid inclusions. The previously estimated high pressures above 6 kbar are the results of the misinterpretation of the fluid inclusion assemblages. Our study further attest that most of the carbonatites worldwide are rather carbothermal than primary in origin.

(iv) Stable C-O and noble gas isotope data indicate the primary mantle origin of the fluid inclusions and their host mineral phases. The least altered samples reveal a mixed DMM and plume origin of the carbonatites. Admixture of a SCLM component into the source cannot be confirmed based on the available data.

(v) The off-axis position and the plume–DMM-like origin of the complexes indicate that a low-viscosity carbonatite liquid ascended relatively rapidly in the early stage of the rift formation of the East African Superplume along deeply rooted fault zones, thus limiting a possibility for the carbonatitic magma to mix with the continental lithosphere.

(vi) Owing to the rapid ascent, the depleted DMM and plume sources no significant strategic/precious element concentration was observed in the samples. The occurrence of minor sulfide might be related to the hydrothermal fluids expelled from the carbonatite magma. Recrystallization phenomena as well as elevated P_2O_5 concentrations imply hydrothermal remobilization under sub-solidus conditions that resulted in apatite enrichment in some samples.

Declaration of Competing Interest

The authors declare that they have no known competing financial interests or personal relationships that could have appeared to influence the work reported in this paper.

Acknowledgements

The research was supported by the Czech Science Foundation projects 15-08583S and 19-29124X. The research was supported by the European Union and the State of Hungary, co-financed by the European Regional Development Fund in the project of GINOP-2.3.2-15–2016-00009 ‘ICER’. Zsolt Benkó acknowledges the financial support of the János Bolyai research scholarship of the Hungarian Academy of Sciences. We thank Ivana Jačková for assistance with C-O isotope analyses at CGS. The authors are indebted to Félix Schubert and Tivadar M. Tóth for the access to the microthermometry lab of the University of Szeged. The authors are grateful to Jens Hopp, Tobias Fischer and the anonymous reviewer, whose comments and suggestions significantly helped to improve and clarify this manuscript.

References

Ackerman, L., Magna, T., Rapprich, V., Upadhyay, D., Krátký, O., Čejková, B., Erban, V., Kochergina, Y.V., Hrstka, T., 2017. Contrasting petrogenesis of spatially related carbonatites from Samalpatti and Sevattur, Tamil Nadu, India. Lithos 284–285, 257–275. https://doi.org/10.1016/j.lithos.2017.03.029.

Ackerman, L., Rapprich, V., Polák, L., Magna, T., McLemore, V.T., Pour, O., Čejková, B., 2021. Petrogenesis of silica-rich carbonatites from continental rift settings: a missing link between carbonatites and carbonated silicate melts? J. Geosci. (Czech Republic). https://doi.org/10.3190/jgeosci.320.

Alvin, M.P., Dunphy, J.M., Groves, D.I., 2004. Nature and genesis of a carbonatite-associated fluorite deposit at Speewah, East Kimberley region, Western Australia. Mineral. Petrol. 80, 127–153. https://doi.org/10.1007/s00710-003-0015-3.

Anders, E., Grevesse, N., 1989. Abundances of the elements: meteoritic and solar. Geochim. Cosmochim. Acta 53, 197–214. https://doi.org/10.1016/0016-7037(89)90286-X.

Andersen, T., 1986. Magmatic fluids in the Fen carbonatite complex, S.E. Norway. Contrib. Mineral. Petrol. 93, 491–503. https://doi.org/10.1007/bf00371719.

Ballentine, C.J., Burgess, R., Marty, B., 2002. Tracing fluid origin, transport and interaction in the crust. Rev. Mineral. Geochem. 47 https://doi.org/10.2138/rmg.2002.47.13.

Bell, K., Simonetti, A., 2010. Source of parental melts to carbonatites-critical isotopic constraints. Mineral. Petrol. 98, 77–89. https://doi.org/10.1007/s00710-009-0059-0.

Biggar, G.M., 1967. Apatite compositions and liquidus phase relationships on the join Ca$(OH)_2$-CaF_2-Ca$_3(PO_4)2H_2O$ from 250 to 4000 bars. Mineral. Mag. 36, 539–564. https://doi.org/10.1180/minmag.1967.036.280.08.

Bloomfield, K., 1973. Economic aspects of Uganda carbonatite complexes. Overseas Geol. Miner. Resour. 41, 139–167.

Bodnar, R.J., 1993. Revised equation and table for determining the freezing point depression of H_2O-NaCl solutions. Geochim. Cosmochim. Acta 57, 683–684. https://doi.org/10.1016/0016-7037(93)90378-A.

Bodnar, R.J., Vityk, M.O., 1994. Interpretation of microthermometric data for H_2O-NaCl fluid inclusions. In: De Vivo, B, Frezzotti, ML (Eds.), Fluid inclusions in minerals: methods and applictions. Virginia Polytechnic Inst. State Univ, Blacksburgh, pp. 117–131.

Bowers, T.S., Helgeson, H.C., 1983. Calculation of the thermodynamic and geochemical consequences of nonideal mixing in the system H_2O-CO_2-NaCl on phase relations in geologic systems: Equation of state for H_2O-CO_2-NaCl fluids at high pressures and temperatures. Geochim. Cosmochim. Acta 47, 1247–1275. https://doi.org/10.1016/0016-7037(83)90066-2.

Broom-Fendley, S., Styles, M.T., Appleton, J.D., Gunn, G., Wall, F., 2016. Evidence for dissolution-reprecipitation of apatite and preferential LREE mobility in carbonatite-derived late-stage hydrothermal processes. Am. Mineral. 101, 596–611. https://doi.org/10.2138/am-2016-5502CCBY.

Buikin, A.I., Verchovsky, A.B., Sorokhtina, N.V., Kogarko, L.N., 2014. Composition and sources of volatiles and noble gases in fluid inclusions in pyroxenites and carbonatites of the Seblyavr Massif, Kola Peninsula. Petrology 22, 507–520. https://doi.org/10.1134/S0869591114050038.

Chakhmouradian, A.R., Reguir, E.P., Zaitsev, A.N., Couëslan, C., Xu, C., Kynický, J., Mumin, A.H., Yang, P., 2017. Apatite in carbonatitic rocks: Compositional variation, zoning, element partitioning and petrogenetic significance. Lithos 274–275, 188–213. https://doi.org/10.1016/j.lithos.2016.12.037.

Chen, W., Kamenetsky, V.S., Simonetti, A., 2013. Evidence for the alkaline nature of parental carbonatite melts at Oka complex in Canada. Nat. Commun. 4, 1–6. https://doi.org/10.1038/ncomms3687.

Comin-Chiaramonti, P., Gomes, C., Censi, P., Speziale, S., 2005. Carbonatites from Southeastern Brazil: a model for the carbon and oxygen isotope variations. Mesozoic to Cenozoic alkaline Magmat. Brazilian Platf. 629–649.

Costanzo, A., Moore, K.R., Wall, F., Feely, M., 2006. Fluid inclusions in apatite from Jacupiranga calcite carbonatites: evidence for a fluid-stratified carbonatite magma chamber. Lithos 91, 208–228. https://doi.org/10.1016/j.lithos.2006.03.047.

Courtillot, V., Jaupart, C., Manighetti, I., Tapponnier, P., Besse, J., 1999. On causal links between flood basalts and continental breakup. Earth Planet. Sci. Lett. 166, 177–195. https://doi.org/10.1016/S0012-821X(98)00282-9.

Daëron, M., Drysdale, R.N., Peral, M., Huyghe, D., Blamart, D., Coplen, T.B., Lartaud, F., Zanchetta, G., 2019. Most Earth-surface calcites precipitate out of isotopic equilibrium. Nat. Commun. 10 https://doi.org/10.1038/s41467-019-08336-5.

Davies, K.A., 1965. The Geology of Part of South-East Uganda, with Special Reference to the Alkaline Complexes, Memoire, 8. ed. Geological Survey of Uganda.

de Moor, J.M., Fischer, T.P., King, P.L., Botcharnikov, R.E., Hervig, R.L., Hilton, D.R., Barry, P.H., Mangasini, F., Ramirez, C., 2013. Volatile-rich silicate melts from Oldoinyo Lengai volcano (Tanzania): implications for carbonatite genesis and eruptive behavior. Earth Planet. Sci. Lett. 361, 379–390. https://doi.org/10.1016/j.epsl.2012.11.006.

Deines, P., 1989. Stable isotope variations in carbonatites. In: BelL, K (Ed.), Carbonatites: Genesis and Evolution. Unwyn Hyman, London, pp. 301–359.

Deines, P., Gold, D.P., 1973. The isotopic composition of carbonatite and kimberlite carbonates and their bearing on the isotopic composition of deep-seated carbon. Geochim. Cosmochim. Acta 37, 1709–1733. https://doi.org/10.1016/0016-7037(73)90158-0.

Demény, A., Harangi, S., 1996. Stable isotope studies and processes of carbonate formation in Hungarian alkali basalts and lamprophyres: evolution of magmatic fluids and magma-sediment interactions. Lithos 37, 335–349. https://doi.org/10.1016/0024-4937(95)00029-1.

Demény, A., Ahijado, A., Casillas, R., Vennemann, T.W., 1998. Crustal contamination and fluid/rock interaction in the carbonatites of Fuerteventura (Canary Islands, Spain): A C, O, H isotope study. Lithos 44, 101–115. https://doi.org/10.1016/S0024-4937(98)00050-4.

Demény, A., Sitnikova, M.A., Karchevsky, P.I., 2004. Stable C and O isotope compositions of carbonatite complexes of the Kola Alkaline Province: phoscorite carbonatite relationships and source compositions. In: Wall, F., Zaitsev, A.N. (Eds.), Phoscorites and carbonatites from mantle to mine: the key example of the Kola alkaline province. Mineralogical Society Series. Mineralogical Society of Great Britain and Ireland, London, pp. 407–431.

Dempírová, L., Šikl, J., Kašičková, R., Zoulková, V., Kříbek, B., 2010. The evaluation of precision and relative error of the main components of silicate analyses in Central Laboratory of the Czech Geological Survey. Zprávy o Geol. výzkumech v roce 2009 (27), 326–330.

Dennis, K.J., Schrag, D.P., 2010. Clumped isotope thermometry of carbonatites as an indicator of diagenetic alteration. Geochim. Cosmochim. Acta 74, 4110–4122. https://doi.org/10.1016/j.gca.2010.04.005.

Elliott, H.A.L., Wall, F., Chakhmouradian, A.R., Siegfried, P.R., Dahlgren, S., Weatherley, S., Finch, A.A., Marks, M.A.W., Dowman, E., Deady, E., 2018. Fenites associated with carbonatite complexes: a review. Ore Geol. Rev. 93, 38–59. https://doi.org/10.1016/j.oregeorev.2017.12.003.

Ernst, R.E., Bell, K., 2010. Large igneous provinces (LIPs) and carbonatites. Mineral. Petrol. 98, 55–76. https://doi.org/10.1007/s00710-009-0074-1.

Ferrero, S., Wunder, B., Ziemann, M.A., Wälle, M., O'Brien, P.J., 2016. Carbonatitic and granitic melts produced under conditions of primary immiscibility during anatexis in the lower crust. Earth Planet. Sci. Lett. 454, 121–131. https://doi.org/10.1016/j.epsl.2016.08.043.

Frezzotti, M.L., Tecce, F., Casagli, A., 2012. Raman spectroscopy for fluid inclusion analysis. J. Geochem. Explor. 112, 1–20. https://doi.org/10.1016/j.gexplo.2011.09.009.

Furman, T., 2007. Geochemistry of East African Rift basalts: an overview. J. Afr. Earth Sci. 48, 147–160. https://doi.org/10.1016/j.jafrearsci.2006.06.009.

George, R., Rogers, N., Kelley, S., 1998. Earliest magmatism in Ethiopia: evidence for two mantle plumes in one flood basalt province. Geology 26, 923–926.

Graham, D.W., 2002. Noble gas isotope geochemistry of MORBs and OIBs. In: Porcelli, D., Ballentine, C.J., Wierler, R. (Eds.), Reviews in Mineralogy & Geochemistry, 1st47. Geochemical Society, Mineralogical Society of America, Washington, pp. 247–317.

Green, D.H., Wallace, E.M., 1988. Mantle metasomatism by ephemeral carbonatite melts. Nature 336, 459–462. https://doi.org/10.1038/336459a0.

Groves, D.I., Vielreicher, N.M., 2001. The Phalabowra (Palabora) carbonatite-hosted magnetite-copper sulfide deposit, South Africa: an end-member of the iron-oxide copper-gold-rare earth element deposit group? Mineral. Depos. 36, 189–194. https://doi.org/10.1007/s001260050298.

Guzmics, T., Kodolányi, J., Kovács, I., Szabó, C., Bali, E., Ntaflos, T., 2008. Primary carbonatite melt inclusions in apatite and in K-feldspar of clinopyroxene-rich mantle xenoliths hosted in lamprophyre dikes (Hungary). Mineral. Petrol. 94, 225–242. https://doi.org/10.1007/s00710-008-0014-5.

Guzmics, T., Mitchell, R.H., Szabó, C., Berkesi, M., Milke, R., Abart, R., 2011. Carbonatite melt inclusions in coexisting magnetite, apatite and monticellite in Kerimasi calciocarbonatite, Tanzania: Melt evolution and petrogenesis. Contrib. Mineral. Petrol. 161, 177–196. https://doi.org/10.1007/s00410-010-0525-z.

Guzmics, T., Ratter, K., Berkesi, M., Szabó, C., Mitchell, R.H., Milke, R., 2012. Liquid immiscibility between silicate, carbonate and sulfide melts in melt inclusions hosted in co-precipitated minerals from Kerimasi volcano (Tanzania): evolution of carbonated nephelinitic magma. Contrib. Mineral. Petrol. 164, 101–122. https://doi.org/10.1007/s00410-012-0728-6.

Guzmics, T., Berkesi, M., Bodnar, R.J., Fall, A., Bali, E., Milke, R., Vetlényi, E., Szabó, C., 2019. Natrocarbonatites: a hidden product of three-phase immiscibility. Geology 47, 527–530. https://doi.org/10.1130/G46125.1.

Halldórsson, S.A., Hilton, D.R., Scarsi, P., Abebe, T., Hopp, J., 2014. A common mantle plume source beneath the entire East African Rift System revealed by coupled helium-neon systematics. Geophys. Res. Lett. 41, 2304–2311. https://doi.org/10.1002/2014GL059424.

Hilton, D.R., Halldórsson, S.A., Barry, P.H., Fischer, T.P., De Moor, J.M., Ramirez, C.J., Mangasini, F., Scarsi, P., 2011. Helium isotopes at Rungwe Volcanic Province, Tanzania, and the origin of East African Plateaux. Geophys. Res. Lett. 38, 1–5. https://doi.org/10.1029/2011GL049589.

Hoernle, K., Tilton, G., Le Bas, M.J., Duggen, S., Garbe-Schönberg, D., 2002. Geochemistry of oceanic carbonatites compared with continental carbonatites: Mantle recycling of oceanic crustal carbonate. Contrib. Mineral. Petrol. 142, 520–542. https://doi.org/10.1007/s004100100308.

Hogarth, D.D., 1977. Classification and nomenclature of the pyrochlore group. Am. Mineral. 62, 403–410.

Holland, G., Ballentine, C.J., 2006. Seawater subduction controls the heavy noble gas composition of the mantle. Nature 441, 186–191. https://doi.org/10.1038/nature04761.

Hopp, J., Viladkar, S.G., 2018. Noble gas composition of Indian carbonatites (Amba Dongar, Siriwasan): Implications on mantle source compositions and late-stage hydrothermal processes. Earth Planet. Sci. Lett. 492, 186–196. https://doi.org/10.1016/j.epsl.2018.04.011.

Hopp, J., Trieloff, M., Altherr, R., 2004. Neon isotopes in mantle rocks from the Red Sea region reveal large-scale plume-lithosphere interaction. Earth Planet. Sci. Lett. 219, 61–76. https://doi.org/10.1016/S0012-821X(03)00691-5.

Hou, Z., Liu, Y., Tian, S., Yang, Z., Xie, Y., 2015. Formation of carbonatite-related giant rare-earth-element deposits by the recycling of marine sediments. Sci. Rep. 5, 1–10. https://doi.org/10.1038/srep10231.

Jones, A.P., Wyllie, P.J., 1986. Solubility of rare earth elements in carbonatite magmas, indicated by the liquidus surface in $CaCO_3Ca(OH)_2La(OH)_3$ at 1 kbar pressure. Appl. Geochem. 1, 95–102. https://doi.org/10.1016/0883-2927(86)90040-5.

Jones, A.P., Genge, M., Carmody, L., 2013. Carbonate melts and carbonatites. Rev. Mineral. Geochem. 75, 289–322. https://doi.org/10.2138/rmg.2013.75.10.

Kendrick, M.A., Burnard, P., 2013. Noble gases and halogens in fluid inclusions: a journey through the earth's crust. In: Burnard, P (Ed.), The Noble Gases as Geochemical Tracers. Springer Verlag, Heidelberg, New York, Dordrecht, London, pp. 319–369.

Kennedy, B.M., Hiyagon, H., Reynolds, J.H., 1990. Crustal neon: a striking uniformity. Earth Planet. Sci. Lett. 98, 277–286.

Kjarsgaard, B., 1998. Phase relations of a carbonated high-CaO nephelinite at 0.2 and 0.5 GPa. J. Petrol. 39, 2061–2075.

Kjarsgaard, B.A., Hamilton, D.L., Peterson, T.D., 1995. Peralkaline nephelinite/carbonatite liquid immiscibility: comparison of phase compositions in experiments and natural lavas from Oldoinyo Lengai. In: Bell, K., Keller, J. (Eds.), Carbonatite Volcanism, IAVCEI Proceedings in Volcanology. Springer, Berlin, Heidelberg, pp. 163–190. https://doi.org/10.1007/978-3-642-79182-6_13.

Kresten, P., Morogan, V., 1986. Fenitization at the Fen complex, southern Norway. Lithos 19, 27–42. https://doi.org/10.1016/0024-4937(86)90013-7.

Kumar, A., Charan, S.N., Gopalan, K., Macdougall, J.D., 1998. A long-lived enriched mantle source for two Proterozoic carbonatite complexes from Tamil Nadu, southern India. Geochim. Cosmochim. Acta 62, 515–523. https://doi.org/10.1016/S0016-7037(97)00341-4.

Lee, W.J., Wyllie, P.J., 1998. Petrogenesis of carbonatite magmas from mantle to crust, constrained by the system $CaO-(MgO+FeO^*)-(Na_2O+K_2O)-(SiO_2+Al_2O_3+TiO_2)-CO_2$. J. Petrol. 39, 495–517. https://doi.org/10.1093/petroj/39.3.495.

Lee, J.Y., Marti, K., Severinghaus, J.P., Kawamura, K., Yoo, H.S., Lee, J.B., Kim, J.S., 2006. A redetermination of the isotopic abundances of atmospheric Ar. Geochim. Cosmochim. Acta 70, 4507–4512. https://doi.org/10.1016/j.gca.2006.06.1563.

Leya, I., Wieler, R., 1999. Nucleogenic production of Ne isotopes in Earth's crust and upper mantle induced by alpha particles from the decay of U and Th. J. Geophys. Res. Solid Earth 104, 15439–15450. https://doi.org/10.1029/1999jb900134.

Liu, X., Fleet, M.E., 2009. Phase relations of nahcolite and trona at high P-T conditions. J. Mineral. Petrol. Sci. 104, 25–36. https://doi.org/10.2465/jmps.080402.

Lustrino, M., Luciani, N., Stagno, V., 2019. Fuzzy petrology in the origin of carbonatitic/pseudocarbonatitic Ca-rich ultrabasic magma at Polino (Central Italy). Sci. Rep. 9, 1–14. https://doi.org/10.1038/s41598-019-45471-x.

Lustrino, M., Ronca, S., Caracausi, A., Ventura Bordenca, C., Agostini, S., Faraone, D.B., 2020. Strongly SiO_2-undersaturated, CaO-rich kamafugitic Pleistocene magmatism in Central Italy (San Venanzo volcanic complex) and the role of shallow depth limestone assimilation. Earth-Science Rev. 208, 103256. https://doi.org/10.1016/j.earscirev.2020.103256.

Mackay, D.A.R., Simandl, G.J., 2014. Geology, market and supply chain of niobium and tantalum—a review. Mineral. Depos. 49, 1025–1047. https://doi.org/10.1007/s00126-014-0551-2.
Magna, T., Viladkar, S., Rapprich, V., Pour, O., Hopp, J., Čejková, B., 2020. Nb–V-enriched sövites of the northeastern and eastern part of the Amba Dongar carbonatite ring dike, India – a reflection of post-emplacement hydrothermal overprint? Geochemistry 80, 125534. https://doi.org/10.1016/j.chemer.2019.125534.
Markl, G., Baumgartner, L., 2002. pH changes in peralkaline late-magmatic fluids. Contrib. Mineral. Petrol. 144, 331–346. https://doi.org/10.1007/s00410-002-0401-6.
Mata, J., Manuel, M., Doucelance, R., Ader, M., Silva, L.C., 2010. Noble gas and carbon isotopic signatures of Cape Verde oceanic carbonatites: Implications for carbon provenance. Earth Planet. Sci. Lett. 291, 70–83. https://doi.org/10.1016/j.epsl.2009.12.052.
McCrea, J.M., 1950. On the isotopic chemistry of carbonates and a paleotemperature scale. J. Chem. Phys. 18 (6), 849–857. https://doi.org/10.1063/1.1747785.
McDonald, A., Murray, G., Wertz, M., 2010. Sukulu Phosphate Project Scoping. Study report 1–10.
McDonough, W.F., Sun, S.s., 1995. The composition of the Earth. Chem. Geol. 120, 223–253. https://doi.org/10.1016/0009-2541(94)00140-4.
Mitchell, R.H., 2005. Carbonatites and carbonatites and carbonatites. Can. Mineral. 43, 2049–2068. https://doi.org/10.2113/gscanmin.43.6.2049.
Mollex, G., Füri, E., Burnard, P., Zimmermann, L., Chazot, G., Kazimoto, E.O., Marty, B., France, L., 2018. Tracing helium isotope compositions from mantle source to fumaroles at Oldoinyo Lengai volcano, Tanzania. Chem. Geol. 480, 66–74. https://doi.org/10.1016/j.chemgeo.2017.08.015.
Moreira, M., Staudacher, T., Sarda, P., Schilling, J.G., Allègre, C.J., 1995. A primitive plume neon component in MORB: the Shona ridge-anomaly, South Atlantic (51-52°S). Earth Planet. Sci. Lett. 133, 367–377. https://doi.org/10.1016/0012-821X(95)00080-V.
Morogan, V., Martin, R.F., 1985. Mineralogy and partial melting of fenitized crustal xenoliths in the Oldoinyo Lengai carbonatitic volcano, Tanzania. Am. Mineral. 70, 1114–1126.
Murty, S.V.S., Basu, S., Kumar, A., 2007. Noble gases in South Indian carbonatites: trapped and in situ components. J. Asian Earth Sci. 30, 154–169. https://doi.org/10.1016/j.jseaes.2006.08.004.
Nadeau, O., Stevenson, R., Jébrak, M., 2016. Evolution of Montviel alkaline-carbonatite complex by coupled fractional crystallization, fluid mixing and metasomatism - part I: petrography and geochemistry of metasomatic aegirine-augite and biotite: implications for REE-Nb mineralization. Ore Geol. Rev. 72, 1143–1162. https://doi.org/10.1016/j.oregeorev.2015.09.022.
Nasraoui, M., Bilal, E., 2000. Pyrochlores from the Lueshe carbonatite complex (Democratic Republic of Congo): a geochemical record of different alteration stages. J. Asian Earth Sci. 18, 237–251. https://doi.org/10.1016/S1367-9120(99)00056-5.
Nelson, D.R., Chivas, A.R., Chappell, B.W., McCulloch, M.T., 1988. Geochemical and isotopic systematics in carbonatites and implications for the evolution of ocean-island sources. Geochim. Cosmochim. Acta 52, 1–17. https://doi.org/10.1016/0016-7037(88)90051-8.
Notholt, A.J., Sheldon, R.P., Davidson, D.F., 1989. The Sukuku phosphate deposits, south-eastern Uganda. Phosphate Deposits of the World. Phosphate Rock Resources, 2. Cambridge University press, Cambridge, pp. 184–186.
Palmer, D.A.S., Williams-Jones, A.E., 1996. Genesis of the carbonatite-hosted fluorite deposit at Amba Dongar, India: evidence from fluid inclusions, stable isotopes, and whole rock-mineral geochemistry. Econ. Geol. 91, 934–950. https://doi.org/10.2113/gsecongeo.91.5.934.
Poutiainen, M., 1995. Fluids in the Siilinjarvi carbonatite complex, eastern Finland: fluid inclusion evidence for the formation conditions of zircon and apatite. Bull. Geol. Soc. Finl. 67, 3–18. https://doi.org/10.17741/bgsf/67.1.001.
Raja, P.K., Vise, J.B., 1973. Paleomagnetism of the Tororo Ring complex, S.E. Uganda. Earth Planet. Sci. Lett. 19, 438–442.
Rankin, A.H., 1977. Fluid-inclusion evidence for the formation conditions of apatite from the Tororo carbonatite complex of eastern Uganda. Mineral. Mag. 41, 155–164. https://doi.org/10.1180/minmag.1977.041.318.02.
Rankin, A.H., Le Bas, M.J., 1974. Nahcolite ($NaHCO_3$) in inclusions in apatites from some E. African ijolites and carbonatites. Mineral. Mag. 39, 564–570. https://doi.org/10.1180/minmag.1974.039.305.09.
Ray, J.S., Ramesh, R., 2006. Stable carbon and oxygen isotopic compositions of Indian carbonatites. Int. Geol. Rev. 48, 17–45. https://doi.org/10.2747/0020-6814.48.1.17.
Ray, J.S., Ramesh, R., Pande, K., Trivedi, J.R., Shukla, P.N., Patel, P.P., 2000. Isotope and rare earth element chemistry of carbonatite-alkaline complexes of Deccan volcanic province: Implications to magmatic and alteration processes. J. Asian Earth Sci. 18, 177–194. https://doi.org/10.1016/S1367-9120(99)00030-9.
Reedman, J.H., 1984. Resources of phosphate, niobium, iron, and other elements in residual soils over the Sukulu carbonatite complex, southeastern Uganda. Econ. Geol. 79, 716–724. https://doi.org/10.2113/gsecongeo.79.4.716.
Roedder, E., 1984. Inclusions in alcalic rock-carbonatite association. In: Ribbe, P.H. (Ed.), Fluid Inclusions, Reviews in Mineralogy. Mineralogical Society of America, Reston, pp. 402–404.
Rogers, N.W., 2006. Basaltic magmatism and the geodynamics of the East African Rift System. Geol. Soc. Spec. Publ. 259, 77–93. https://doi.org/10.1144/GSL.SP.2006.259.01.08.
Roller, S., Wittmann, H., Kastowski, M., Hinderer, M., 2012. Erosion of the Rwenzori Mountains, East African Rift, from in situ-produced cosmogenic ^{10}Be. J. Geophys. Res. Earth Surf. 117 https://doi.org/10.1029/2011JF002117.
Sasada, T., Hiyagon, H., Bell, K., Ebihara, M., 1997. Mantle-derived noble gases in carbonatites. Geochim. Cosmochim. Acta 61, 4219–4228. https://doi.org/10.1016/S0016-7037(97)00202-0.
Scarsi, P., 2000. Fractional extraction of helium by crushing of olivine and clinopyroxene phenocrysts: Effects on the $^3He/^4He$ measured ratio. Geochim. Cosmochim. Acta 64, 3751–3762. https://doi.org/10.1016/S0016-7037(00)00419-1.
Schleicher, H., Kramm, U., Pernicka, E., Schidlowski, M., Schmidt, F., Subramanian, V., Todt, W., Viladkar, S.G., 1998. Enriched subcontinental upper mantle beneath southern India: evidence from Pb, Nd, Sr, and C-O isotopic studies on Tamil Nadu carbonatites. J. Petrol. 39, 1765–1785. https://doi.org/10.1093/petroj/39.10.1765.
Simandl, G.J., 2014. Geology and market-dependent significance of rare earth element resources. Mineral. Deposita 49, 889–904. https://doi.org/10.1007/s00126-014-0546-z.
Simandl, G.J., Paradis, S., 2018. Carbonatites: related ore deposits, resources, footprint, and exploration methods. Appl. Earth Sci. Trans. Inst. Min. Metall. 127, 123–152. https://doi.org/10.1080/25726838.2018.1516935.
Simandl, G.J., Burt, R.O., Trueman, D.L., Paradis, S., 2018. Economic geology models 2. Tantalum and niobium: deposits, resources, exploration methods and market – a primer for geoscientists. Geosci. Can. 45, 85–96. https://doi.org/10.12789/geocanj.2018.45.135.
Sweeney, R.J., 1994. Carbonatite melt compositions in the Earth's mantle. Earth Planet. Sci. Lett. 128, 259–270. https://doi.org/10.1016/0012-821X(94)90149-X.
Taylor, H.P., Frechen, J., Degens, E.T., 1967. Oxygen and carbon isotope studies of carbonatites from the Laacher See District, West Germany and the Alnö District. Sweden. Geochim. Cosmochim. Acta 31, 407–430. https://doi.org/10.1016/0016-7037(67)90051-8.
Ting, W., Burke, E.A.J., Rankin, A.H., Woolley, A.R., 1994a. Characterisation and petrogenetic significance of CO_2, H_2O and CH_4 fluid inclusions in apatite from the Sukulu carbonatite, Uganda. Eur. J. Mineral. 6, 787–803.
Ting, W., Rankin, A.H., Woolley, A.R., 1994b. Petrogenetic significance of solid carbonate inclusions in apatite of the Sukulu carbonatite, Uganda. Lithos 31, 177–187. https://doi.org/10.1016/0024-4937(94)90008-6.
Trieloff, M., Kunz, J., 2005. Isotope systematics of noble gases in the Earth's mantle: possible sources of primordial isotopes and implications for mantle structure. Phys. Earth Planet. Inter. 148, 13–38. https://doi.org/10.1016/j.pepi.2004.07.007.
Trieloff, M., Kunz, J., Clague, D.A., Harrison, D., Allègre, C.J., 2000. The nature of pristine noble gases in mantle plumes. Science 288(5468), 1036–1038. https://doi.org/10.1126/science.288.5468.1036.
Trubač, J., Magna, T., Čejková, B., Vondrovicová, L., Rapprich, V., 2019. Rapid determination of carbon isotope composition in carbonatites using isotope ratio mass spectrometry – comparison of dual-inlet, elemental-analyzer and continuous-flow techniques. Rapid Commun. Mass Spectrom. 33, 1355–1362. https://doi.org/10.1002/rcm.8482.
Trull, T.W., Kurz, M.D., 1993. Experimental measurements of ^3He and ^4He mobility in olivine and clinopyroxene at magmatic temperatures. Geochim. Cosmochim. Acta 57, 1313–1324. https://doi.org/10.1016/0016-7037(93)90068-8.
Valbracht, P.J., Staudacher, T., Malahoff, A., Allègre, C.J., 1997. Noble gas systematics of deep rift zone glasses from Loihi Seamount. Hawaii. Earth Planet. Sci. Lett. 150, 399–411. https://doi.org/10.1016/s0012-821x(97)00094-0.
Valkiers, S., Schaefer, F., Debièvre, P., 1994. Near-absolute gas(isotope) mass spectrometry: isotope abundance(and atomic weight) determinations of neon, krypton, xenon and argon. Elsevier, Amsterdam.
Verplanck, P.L., Mariano, A.N., Mariano, A.J., 2016. Rare earth element ore geology of carbonatites. Rev. Econ. Geol. 18, 5–32. https://doi.org/10.5382/Rev.18.01.
Viladkar, S.G., Gittins, J., 2016. Trace elements and REE geochemistry of Siriwasan carbonatite, Chhota Udaipur, Gujarat. J. Geol. Soc. India 87, 709–715. https://doi.org/10.1007/s12594-016-0443-4.
Woolley, A.R., Kempe, D.R.C., 1989. Carbonatites: nomenclature, average chemical compositions, and element distribution. In: Bell, K. (Ed.), Carbonatites, Genesis and Evolution. Unwin Hyman, London, pp. 1–14.
Woolley, A.R., Kjarsgaard, B.A., 2008. Paragenetic types of carbonatite as indicated by the diversity and relative abundances of associated silicate rocks: evidence from a global database. Can. Mineral. 46, 741–752. https://doi.org/10.3749/canmin.46.4.741.
Wyllie, P.J., 1966. Experimental studies of carbonatite problems: the origin and differentiation of carbonatite magmas. In: Gittins, J. (Ed.), Carbonatites. Intersicene Publishers, New York, pp. 311–352.
Xue, L., Gani, N.D., Abdelsalam, M.G., 2019. Drainage incision, tectonic uplift, magmatic activity, and paleo-environmental changes in the Kenya Rift, East African Rift System: a morpho-tectonic analysis. Geomorphology 345, 106839. https://doi.org/10.1016/j.geomorph.2019.106839.
Zurevinski, S.E., Mitchell, R.H., 2004. Extreme compositional variation of pyrochlore-group minerals at the Oka carbonatite complex, Quebec: evidence of magma mixing? Can. Mineral. 42, 1159–1168. https://doi.org/10.2113/gscanmin.42.4.1159.